2015

Broadband Electrical Detection of Individual Biological Cells

Yaqing Ning
Lehigh University

Broadband Electrical Detection of Individual Biological Cells

by

Yaqing Ning

Presented to the Graduate and Research Committee

of Lehigh University

in Candidacy for the Degree of

Doctor of Philosophy

in

Electrical Engineering

Lehigh University

May 2015

Approved and recommended for acceptance as a dissertation in partial fulfillment of the requirements for the degree of Doctor of Philosophy.

_____

Date

_____

Dr. James C.M. Hwang, Dissertation Advisor, Chair

_____

Accepted Date

Committee Members:

_____

Dr. Miltiadis Hatalis

_____

Dr. Svetlana Tatic-Lucic

_____

Dr. Xuanhong Cheng

_____

Dr. Cristiano Palego

Acknowledgements

I would like to greatly thank my Ph.D advisor, Dr. James C.M. Hwang, who leads me all the way to be an independent researcher with critical thinking and open mind. He guided and inspired me tremendously in my academic research. All the philosophy that I learned from him about both academic and personal life will light my way in the future.

I would like to thank all my committee members: Dr. Miltiadis Hatalis, Dr. Svetlana Tatic-Lucic, Dr. Xuanhong Cheng, and Dr. Cristiano Palego, for their insightful suggestions, and challenges as well, to stimulate my thinking. A special thanks goes to Dr. Palego, who is more than a mentor and a friend, who guided me throughout my PhD training.

Working with all my colleagues in the Compound Semiconductor Technology Laboratory (CSTL) group is a pleasure. Dr. David Molinero, Dr. Subrata Halder, Dr. Renfeng Jin, Dr. Weike Wang, Dr. Guanghai Ding, Xi Luo, Vahid Gholizadeh, Xiao Ma, Mohammad Javad Asadi, Yaghoob Rahbarihagh, Kuanchen Xiong, thanks for always being so kind and generous in helping me. I am also grateful to Caroline Multari, who never hesitate to share her knowledge with me during our collaboration on the project. Dr. Caterina Merla and Dr. Agnese Denzi had valuable contributions to my research. I also received great help from the former group members as well: Dr. Francesco Solazzi, Dr. Chen Cheng, Dr. Mikhail Shirokov and Dr. Jianwen Bao. They showed their support in different ways.

I would like to acknowledge Dr. Chuck Goldsmith and Derek Scarbrough at MEMtronics Corp. for their support and help in my research on the RF MEMS switch and

phase shifter, also Dr. Kathleen Muhonen who was my mentor during my summer internship at RFMD, for her guidance in the industry trail.

I am grateful for all my friends at Lehigh, particularly to Dr. Beibei Zeng and Le Zhao, who were always supportive through my courses, research and life. Thanks go to Dr. Yadan Tang, Dr. Peng Cheng, Qianying Guo, Dr. Yang Liu, Cong Liu, Long Xu, Jin Wang, Ling Ju, Dan You, Chao Zhao, Liping Pan, Yajing Chen, Linlin Fan, Zhuang Cai, etc., who shared all the happiness and tears together with me like my family.

I receive strong support from my parents, Jinling Cao and Jinwei Ning, who are willing to teach me their life experiences and are patient enough to witness my progress and milestones in my life. Finally I would like to thank Shihong Fang, who loves, cares, and respects me always.

There are too many people I need to express my gratitude and words are not enough. Thank you all for being there for me. I really appreciate all your help. Without you, my PhD could not be completed.

Table of Contents

List of Tables

List of Figures

Abstract

Unlike traditional methods of cell detection which accomplished through chemical or optical means, electrical cell detection can be label-free and nondestructive with high throughput. Broadband electrical detection can have additional advantages. For example, based on the different dispersion characteristics, live and dead cells can be differentiated at MHz frequencies, cell types can be identified at GHz frequencies, and surface functionality can be detected at THz frequencies.

To resolve the dilemma encountered by Coulter counters and to evolve a general-purpose electrical detection technique, broadband microwave measurement is used to overcome electrode polarization, AC dielectrophoresis to precisely place cells between narrowly spaced electrodes for maximum cell-to-sample volume ratio, and relatively wide microfluidic channels to prevent cell clogging. This thesis work mainly presents detailed data and analysis at higher frequencies (GHz vs. MHz) to prove that the unique combination of these approaches can be reproducibly sensitive to single cells of different types. The electric circuit model that generated from different electrode designs of CPW and CPS consistently extracts the same value for the resistance of the cytoplasm. Furthermore, simple analysis of the data confirms that microwave signals can penetrate through the cell membrane to probe the properties of cytoplasm.

Chapter 1. Introduction

1.1. Microwave in Biomedical Applications

Health care is becoming a global problem with increasing attention these years. Efforts have been made to improve quality of care or fight against diseases. The National Academy of Engineering has defined health care as one of the significant challenges for engineering. RF and microwave technologies certainly play critical roles in fighting with the challenges and make more affordable and functional health care. The use of microwaves in medical applications is growing rapidly in different fields: surgery and treatment of tissues[1][2][3], wireless communication and power transfer for implants[4][5][6], microwave imaging for breast cancer[7][8][9], understanding of cell topography and architecture[10][11], etc.

Conventionally, RF and microwave systems are designed for homogeneous, isotropic and linear media where the environment for wave propagation do not change. However, under the biomedical background, to utilize the microwave is very challenging with the consideration of realistic issues. The RF-field interactions with the biological systems demonstrated by Schwan [12] show the frequency dependency and translate into relaxation. The three major dispersions of biomaterial are indicated in Fig. 1.1. α-dispersion is due to ionic diffusion process of the folded inner membrane system of the cell. β-dispersion is due to Maxwell-Wagner polarization effects where cellular membrane are charged or orientation of permanent dipoles. γ-dispersion is due to the orientation relaxation of water. For the past decades, cytometry that worked in the low-frequency range

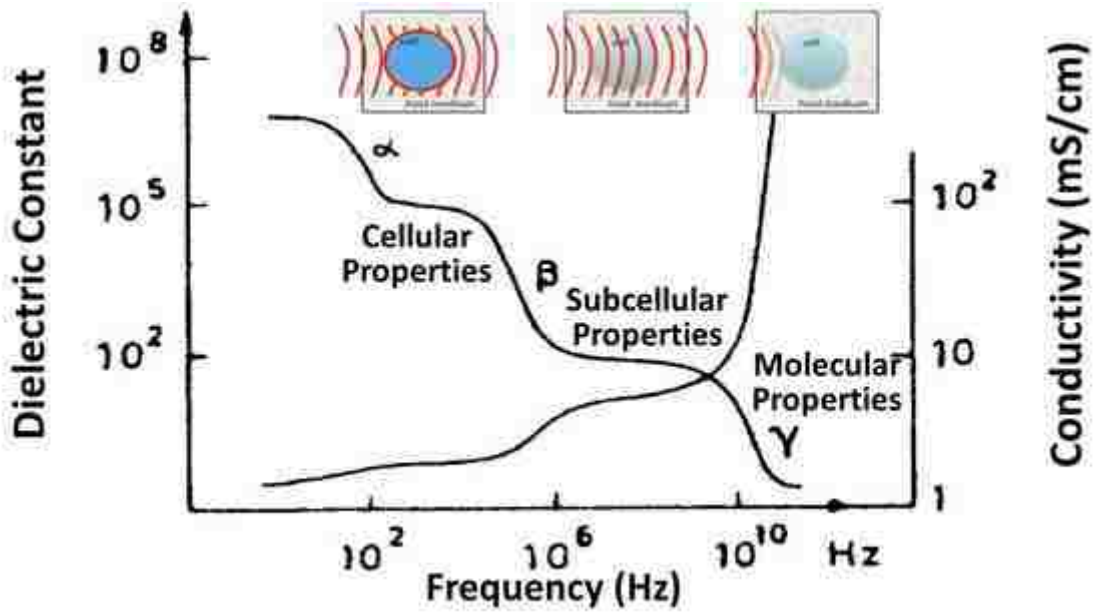

Fig. 1.1 Dielectric constant ε versus frequency and the three major dispersions.

(KHz-MHz) has been leading the research on the cellular level [13][14]. By increasing the frequency into GHz range, the γ-dispersion plays a key role and the most well-known dielectric relaxation is water at 20GHz. Microwave biosensing at GHz range provides additional information to study the broadband dielectric property at cell level, according to different dispersive situation.

1.2. Problem and Challenging

High-performance biological cell detection at single cell level are needed for future bio-detection and bio-surveillance. Traditionally, cell detection is accomplished through chemical or optical means for which sophisticated instruments such as DNA sequencers or flow cytometers are commercially available. DNA sequencers can be very specific, but are slow and destructive. Optical cytometers can be fast and sensitive to single cells and their vitality, but often require labeling which may alter their physiological state [15]. In comparison, electrical cell detection can be label-free and nondestructive with high

throughput. To this end, cytometers capable of measuring the electrical properties of single cells are also commercially available as Coulter counters [16]. However, they can suffer from problems like the dilemma of cell clogging, solution parasitics, etc [17]. Cell clogging occurs if a narrow channel is used to increase the cell-to-sample volume ratio, whereas solution parasitics are aggravated if a wide channel is used to prevent cell clogging. Additionally, Coulter counters typically use discrete frequencies on the order of MHz or lower, which made them unduly sensitive to the size and shape variations of individual cells, as well as the polarization layers formed in the solution between the cells and electrodes [17]. For these reasons, Coulter counters are usually optimized for a special purpose such as for counting human blood cells.

Recently, to resolve the dilemma encountered by Coulter counters and to evolve a general-purpose electrical detection technique, broadband microwave measurement [18] is used to overcome electrode polarization, AC dielectrophoresis to precisely place cells between narrowly spaced electrodes for maximum cell-to-sample volume ratio, and relatively wide microfluidic channels to prevent cell clogging.

Broadband electrical detection can have additional advantages. For example, based on the different dispersion characteristics[19], live and dead cells can be differentiated at MHz frequencies, cell types can be identified at GHz frequencies, and surface functionality can be detected at THz frequencies. As such, broadband electrical detection can yield a wealth of information. However, many challenges remain for broadband electrical detection, such as impedance matching, calibration, modeling, and data analysis described in the following.

Broadband electrical detection of single cells involves measurements highly mismatched in both size and impedance. Typically, broadband transmission lines approximately 100-μm wide are used [20], which require careful transition down to micrometers to match the cell size. At microwave frequencies, the capacitance of the cell membrane (~1 pF) [21] is largely bypassed, so that the electrical properties of the cell are dominated by the cytoplasm resistance (~10^5 Ω) [22], which is much higher than the characteristic impedance (Z0 = 50 Ω) of most microwave measurement systems. Therefore, it is critical for organizations such as National Institute of Standards and Technology to continue to refine the calibration techniques for reproducible detection of nanoliter liquids [23]. It is especially critical in broadband detection for which the signal-to-noise ratio is usually much lower than that of narrowband resonance [24] or interference [25] techniques.

Cells need to be kept alive in solutions which tend to absorb microwave signals. Therefore, microfluidics must be used to minimize the solution volume while delivering cells smoothly. Cell trapping either mechanically [10] or electrically [26] between the detection electrodes maximizes the cell-to-sample volume ratio while allowing relatively wide microfluidic channels to be used to prevent clogging. Whereas electrical trapping does not perturb fluid flow as much as mechanical trapping does, in both cases, the trapped cell can be repeatedly sampled to increase the signal-to-noise ratio.

Although cell trapping can result in high cell-to-sample volume ratios, it is still necessary to characterize the supernatant solution and to de-embed its parasitic effect from the measured data [27]. In fact, using the broadband over-determined data and sophisticated modeling, electrical characteristics of subcellular structures may be extracted

[28][29][30]. Additional complications can be caused by solution conductivity, which can be minimized by resuspending cultured cells in isotonic solutions such as sucrose. However, as cells die, they may release ions into the solution making it again conductive. This can be prevented by a continuous flow to wash away the ions as they are released.

1.3. Cellular Microwave-Based Biosensors

To reach down to the single cell level over a wide frequency band is challenging, considering that one single cell is in considerably small volume over the liquid volume even with the use of microfluidic channel. There are also under-studied parasitics resulting from the liquid environment, the interfaces between different materials, electrode polarization, etc. Studies on the cell liquid environment have been shown in Fig. 1.2.

Broadband electrical detection at or near the single-cell level has recently been

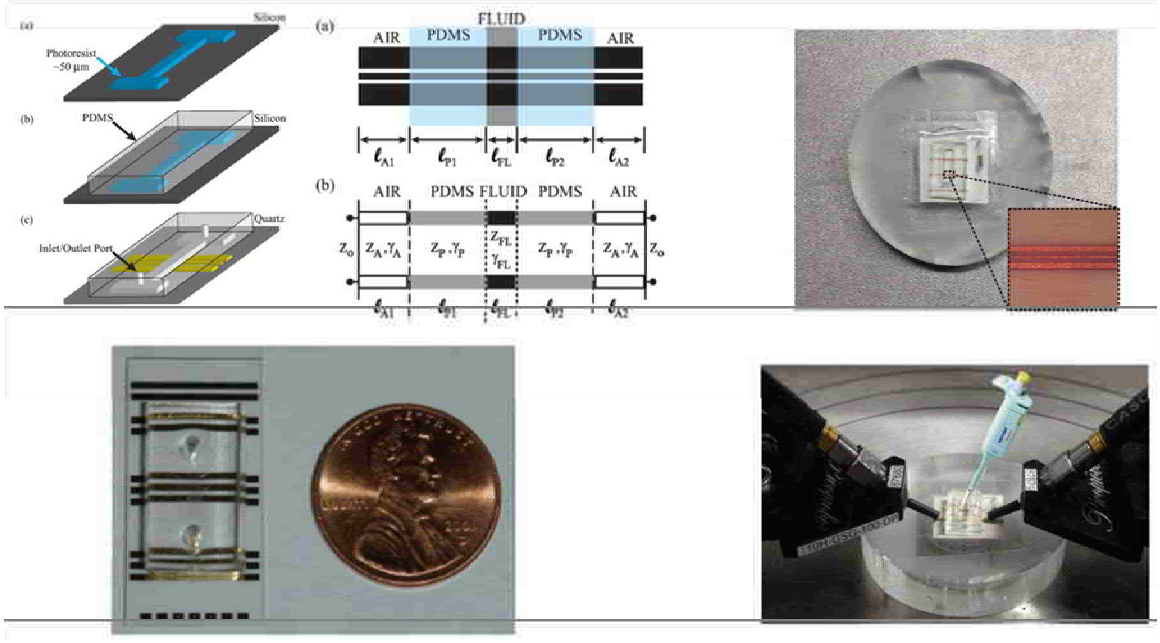

(a) (b)

Fig. 1.3 Examples of integration of electrical detection together with microfluidic channels [23][31].

demonstrated [10][26] shown in Fig. 1.3. The former consists of a coplanar transmission waveguide with a capacitive gap located at the center of the sensor. And the maximum capacitive contrast is obtained around 5GHz with a value close to 0.5 – 0.6 fF. The latter one used a microchamber formed between a gold coplanar waveguide fabricated on a quartz slide. Tests on Jurkat cells in both time and frequency domains showed that live cells had lower resistance but higher capacitance than that of dead cells.

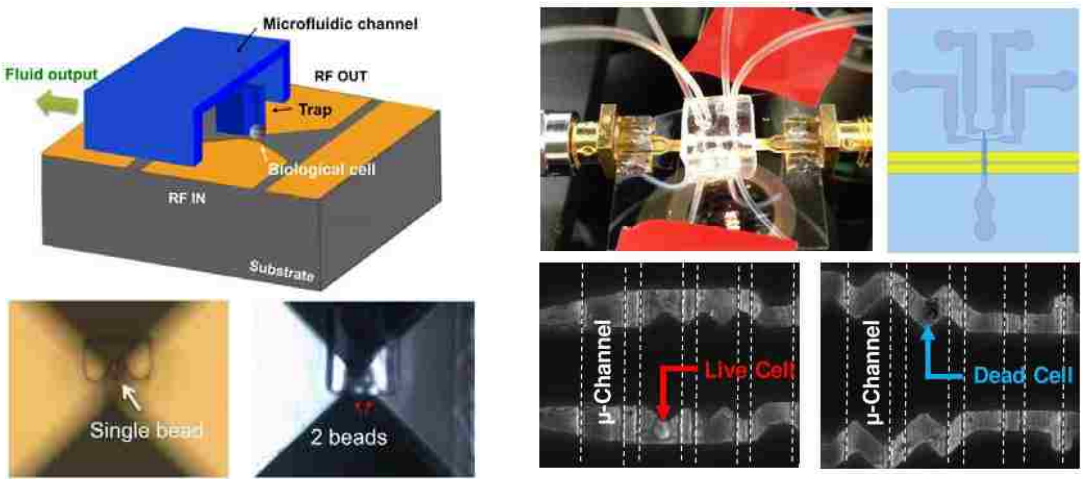

(a) (b)

Fig. 1.4 Examples of electrical detection at or near single-cell level [10][26].

1.4. Motivation

To illustrate how the above-described approaches may be used to overcome the challenges for broadband detection, this dissertation presents a novel microwave microchamber with broadband impedance match and low loss. The microchamber has an integrated microfluidic channel that is capable of delivering single cells, which can then be precisely trapped by dielectrophoresis. The microchamber demonstrates the sensitivity and reproducibility of electrical detection of individual biological cells.

1.5. Organization of the Dissertation

The organization of the dissertation is as follows. In Chapter 2, the design of the microchamber is presented, including electrodes design based on coplanar waveguide and coplanar stripline structure, the utilization of dielectrophoresis force for cell trapping, the integration of the electrodes and microfluidic channel, the preparation of biological cells with its medium, followed by consideration of frequency-dependent material. In Chapter 3, the detection techniques and setups using frequency domain in the range of KHz – MHz with impedance analyzer and using time domain of nanosecond pulse signal are reported. Results show a differentiation of the live and dead cells respectively. After that, demonstration of the broadband electrical detection of biological cells are presented in Chapter 4. The results show that the measured S-parameter dispersions are proportional to the number of cells trapped in the sensing region. The sensitivity and reproducibility are confirmed by the results for cells cultured and trapped in different months, on different test structures. Another improved broader band detection method based on wafer-probing is also demonstrated. Finally, the conclusions of this dissertation and recommendations for future research are discussed in Chapter 5.

References

[1] M. Lazebnik, D. Popovic, L. McCartney, C. B. Watkins, M. J. Lindstrom, J. Harter, S. Sewall, T. Ogilvie, A. Magliocco, T. M. Breslin, W. Temple, D. Mew, J. H. Booske, M. Okoniewski, and S. C. Hagness, "A large-scale study of the ultrawideband microwave dielectric properties of normal, benign and malignant breast tissues obtained from cancer surgeries.," Phys. Med. Biol., vol. 52, no. 20, pp. 6093–115, Oct. 2007.

[2] E. R. Ward and B. Stroy, "A review of dielectric properties of normal and malignant breast tissue," in Proceedings IEEE SoutheastCon 2002 (Cat. No.02CH37283), 2002, pp. 457–462.

[3] A. P. O'Rourke, M. Lazebnik, J. M. Bertram, M. C. Converse, S. C. Hagness, J. G. Webster, and D. M. Mahvi, "Dielectric properties of human normal, malignant and cirrhotic liver tissue: in vivo and ex vivo measurements from 0.5 to 20 GHz using a precision open-ended coaxial probe.," Phys. Med. Biol., vol. 52, no. 15, pp. 4707–19, Aug. 2007.

[4] A. K. Ramrakhyani, S. Mirabbasi, and Mu Chiao, "Design and optimization of resonance-based efficient wireless power delivery systems for biomedical implants.," IEEE Trans. Biomed. Circuits Syst., vol. 5, no. 1, pp. 48–63, Feb. 2011.

[5] A. Yakovlev, S. Kim, and A. Poon, "Implantable biomedical devices: Wireless powering and communication," IEEE Commun. Mag., vol. 50, no. 4, pp. 152–159, Apr. 2012.

[6] S. Smith, T. B. Tang, J. G. Terry, J. T. M. Stevenson, B. W. Flynn, H. M. Reekie, A. F. Murray, A. M. Gundlach, D. Renshaw, B. Dhillon, A. Ohtori, Y. Inoue, and A. J. Walton, "Development of a miniaturised drug delivery system with wireless power transfer and communication.," IET Nanobiotechnol., vol. 1, no. 5, pp. 80–6, Oct. 2007.

[7] E. C. Fear, P. M. Meaney, and M. A. Stuchly, "Microwaves for breast cancer detection?," IEEE Potentials, vol. 22, no. 1, pp. 12–18, Feb. 2003.

[8] N. Nikolova, "Microwave Imaging for Breast Cancer," IEEE Microw. Mag., vol. 12, no. 7, pp. 78–94, Dec. 2011.

[9] E. C. Fear, X. Li, S. C. Hagness, and M. A. Stuchly, "Confocal microwave imaging for breast cancer detection: localization of tumors in three dimensions.," IEEE Trans. Biomed. Eng., vol. 49, no. 8, pp. 812–22, Aug. 2002.

[10] T. Chen, F. Artis, D. Dubuc, J. J. Fournié, M. Poupot, and K. Grenier, "Microwave biosensor dedicated to the dielectric spectroscopy of a single alive biological cell in its culture medium," in IEEE MTT-S International Microwave Symposium Digest, 2013, pp. 1–4.

[11] Y. Ning, C. Multari, X. Luo, C. Palego, X. Cheng, J. C. M. Hwang, A. Denzi, C. Merla, F. Apollonio, and M. Liberti, "Broadband Electrical Detection of Individual Biological Cells," IEEE Trans. Microw. Theory Tech., vol. 62, no. 9, pp. 1905–1911, Sep. 2014.

[12] H. Schwan, "Determination of biological impedances," Phys. Tech. Biol. Res., vol. 6, pp. 323–406, 1963.

[13] S. Gawad, K. Cheung, U. Seger, A. Bertsch, and P. Renaud, "Dielectric spectroscopy in a micromachined flow cytometer: theoretical and practical considerations," Lab A Chip - LAB CHIP, vol. 4, no. 3, pp. 241–251, 2004.

[14] X. Cheng, Y. Liu, D. Irimia, U. Demirci, L. Yang, L. Zamir, W. R. Rodríguez, M. Toner, and R. Bashir, "Cell detection and counting through cell lysate impedance spectroscopy in microfluidic devices.," Lab Chip, vol. 7, no. 6, pp. 746–55, Jun. 2007.

[15] H. M. Shapiro, "The evolution of cytometers.," Cytometry. A, vol. 58, no. 1, pp. 13–20, Mar. 2004.

[16] T. Sun and H. Morgan, "Single-cell microfluidic impedance cytometry: a review," Microfluid. Nanofluidics, vol. 8, no. 4, pp. 423–443, Mar. 2010.

[17] H. P. Schwan, "Electrode polarization impedance and measurements in biological materials," Ann. New York Acad. Sci., vol. 148, no. A1, pp. 191–209, Feb. 1968.

[18] Y. Ning, C. R. Multari, X. Luo, C. Merla, C. Palego, X. Cheng, and J. C. M. Hwang, "Fast, compact and label-free electrical detection of live and dead single cells," in Proc. IEEE MTT-S International Microwave Workshop Series RF and Wireless Technologies Biomedical and Healthcare Applications, 2013, pp. 1–3.

[19] H. P. Schwan, "Analysis of Dielectric Data: Experience Gained with Biological Materials," IEEE Trans. Electr. Insul., vol. EI-20, no. 6, pp. 913–922, Dec. 1985.

[20] K. Grenier, D. Dubuc, T. Chen, F. Artis, T. Chretiennot, M. Poupot, and J. J. Fournie, "Recent advances in microwave-based dielectric spectroscopy at the cellular level for cancer investigations," IEEE Trans. Microw. Theory Tech., vol. 61, no. 5, pp. 2023–2030, May 2013.

[21] H. Fricke, "The electric capacity of suspensions of red corpuscles of a dog," Phys. Rev., vol. 26, no. 5, pp. 682–687, Nov. 1925.

[22] K. Foster and H. Schwan, "Dielectric properties of tissues and biological materials: a critical review," Crit. Rev. Biomed. Eng., vol. 17, no. 1, pp. 25–104, 1989.

[23] J. C. Booth, N. D. Orloff, J. Mateu, M. Janezic, M. Rinehart, and J. A. Beall, "Quantitative Permittivity Measurements of Nanoliter Liquid Volumes in Microfluidic Channels to 40 GHz," IEEE Trans. Instrum. Meas., vol. 59, no. 12, pp. 3279–3288, Dec. 2010.

[24] L. Y. Zhang, C. Bounaix Morand du Puch, C. Dalmay, A. Lacroix, A. Landoulsi, J. Leroy, C. Mélin, F. Lalloué, S. Battu, C. Lautrette, S. Giraud, A. Bessaudou, P. Blondy, M. O. Jauberteau, and A. Pothier, "Discrimination of colorectal cancer cell lines using microwave biosensors," Sensors Actuators A Phys., vol. 216, pp. 405–416, Sep. 2014.

[25] Y. Yang, H. Zhang, J. Zhu, G. Wang, T. Tzeng, and X. Xuan, "Distinguishing the viability of a single yeast cell with an ultra-sensitive radio frequency sensor," Lab Chip, vol. 10, pp. 553–555, 2010.

[26] C. Palego, C. Merla, Y. Ning, C. R. Multari, X. Cheng, D. G. Molinero, G. Ding, X. Luo, and J. C. M. Hwang, "Broadband microchamber for electrical detection of live and dead biological cells," in 2013 IEEE MTT-S International Microwave Symposium Digest, 2013, pp. 1–3.

[27] Yaqing Ning, C. Multari, Xi Luo, C. Palego, D. Molinero, Xuanhong Cheng, J. C. M. Hwang, and C. Merla, "Coplanar stripline microchamber for electrical detection of live and dead biological cells," in Proc. Euporpean Microwave Conference, 2013, pp. 475–478.

[28] C. Merla, a Denzi, a Paffi, M. Casciola, G. d'Inzeo, F. Apollonio, and M. Liberti, "Novel passive element circuits for microdosimetry of nanosecond pulsed electric fields.," IEEE Trans. Biomed. Eng., vol. 59, no. 8, pp. 2302–11, Aug. 2012.

[29] A. Denzi, C. Merla, C. Palego, F. Apollonio, J. C. M. Hwang, and M. Liberti, "Single Cell Microdosimetric Studies Comparing Ideal and Measured Nanosecond Pulsed Electric Fields," in IEEE MTT-S International Microwave Symposium Digest, 2013, pp. 1–4.

[30] A. Denzi, C. Merla, P. Camilleri, A. Paffi, G. D'Inzeo, F. Apollonio, and M. Liberti, "Microdosimetric Study for Nanosecond Pulsed Electric Fields on a Cell Circuit Model with Nucleus.," J. Membr. Biol., vol. 246, no. 10, pp. 761–767, Apr. 2013.

Chapter 2. Microchamber Design

2.1. Introduction

In order to demonstrate the idea of broad band electrical detection of biological cells, microchambers based on the integration of electrical measurement and microfluidics control must be well designed. In this chapter, the basic principles of the designs are presented.

Section 2.2 presents the characteristics of coplanar waveguide (CPW) including the closed form equations based on the conformal mapping technique. Three-dimensional full-wave finite-element is implemented using commercially-available ANSYS High Frequency Structure Simulator (HFSS). Details of different designs are also discussed. In Section 2.3, the concept and usage of dielectrophoresis (DEP) are presented. DEP takes advantage of the non-uniform electrical field and can be used to trap the biological cells in the target regions. Section 2.4 presents the integration of the electrodes and the microfluidic channel. The fundamentals of biological cells then are discussed in Section 2.5, including the cell culture techniques and the measure-media selection. To an improved accuracy of the test structure, frequency-dependent lossy material must be applied in the electrical simulation to estimate the performance over a wide bandwidth. Hence, Section 2.6 presents the measurement of the frequency-dependent complex permittivity of solution with the use of Keysight (Agilent) 85070E Dielectric Probe. It is important to select the reasonable electrical design and test structure in order to obtain the desired broadband performance.

2.2. Design of Electrodes

2.2.1. Fundamental of Coplanar Waveguide

First proposed by C. P. Wen in 1969 [1], CPW has been widely used in microwave integrated circuits (MICs) as well as monolithic microwave integrated circuits (MMICs) due to its advantages in simplified fabrication, easy shunt configuration of testing, elimination of via holes, small radiation loss over a wide band, and etc [2]. When it comes to the broadband microwave dielectric measurement liquid [3][4][5] or biological cells [6][7][8][9], CPW shows its additional merits. Planar transmission lines can be in contact with test materials non-destructively. CPW benefits from its less dispersive property and can be used for extraction the frequency-dependent material properties. Moreover, the gold material that applied to fabricate the transmission line is bio-compatible and widely used in bio-related experiment [10].

The conventional schematic of a CPW sandwiched between two dielectric substrates is presented in Fig. 2.1. CPW is composed of one center signal line separated by a gap from two ground lines on each side, between the lower and upper partial dielectric region. CPW supports a quasi-TEM mode of propagation. The dimensions of the center strip (W), the gap (S), the dielectric constants of the lower (ε_{r1}) and upper (ε_{r2}) dielectric region determine the characteristic impedance (Z_0), the effective dielectric constant (ε_{eff}) [2] of the line. Assuming infinitely thick lower and upper dielectric region along with semi-infinite ground planes, the properties of CPW lines can be calculated and generated the closed form expressions by conformal mapping techniques:

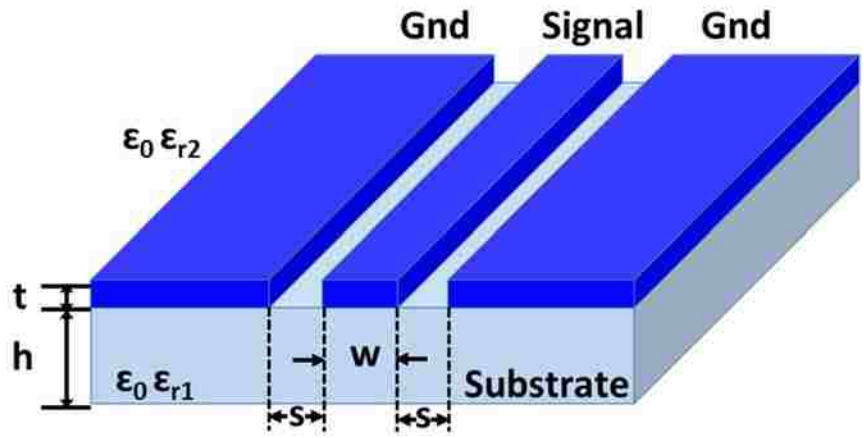

Fig. 2.1 Schematic of a coplanar waveguide structure.

$$\varepsilon_{eff} = \frac{\varepsilon_{r1} + \varepsilon_{r2}}{2} \tag{2.1}$$

$$Z_0 = \frac{30\pi \; K(k_0')}{\sqrt{\varepsilon_{eff}} \; K(k_0)} \tag{2.2}$$

$$k_0 = \frac{S}{S + 2W} \tag{2.3}$$

$$k_0' = \sqrt{1 - k_0^2} \tag{2.4}$$

where $K(k_0)$ is complete elliptic integral of the first kind [2]. Thus, from the measured performances of the transmission line, the dielectric property of the upper dielectric property (ε_{r2}) which is the material-under-test (MUT) can be then extracted.

Besides CPW, there is another planar structure that could be used in the cell detection experiment, which is the coplanar stripline (CPS). CPS is consisted of only two parallel strip conductors separated by a narrow gap [2], shown in Fig. 2.2. CPS is a balanced transmission line where the current on one conductor equals to the current on the other conductor in magnitude but with 180º difference in phase. Thus CPS is good to use in feeding the dipole antenna and balanced mixers. The advantages of using CPS in the cell

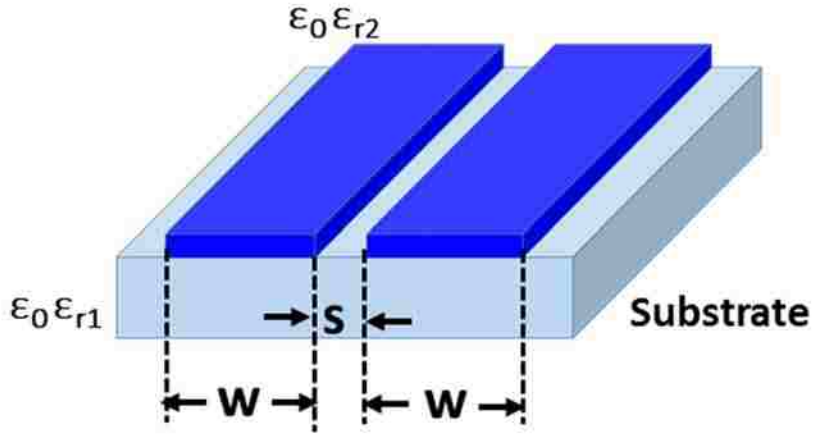

Fig. 2.2 Schematic of a coplanar stripline structure.

measurement is: 1) cells can be trapped in one gap instead of two gaps, which is more suitable for single-cell sensing, 2) parasitic shunt capacitance is reduced and electrical sensitivity is increased, and 3) the total area obscured by the electrodes is reduced, which allows better visual tracking of cell movement in the microfluidic channel.

However, the disadvantages of the CPS are also apparent. Because it lacks a ground plane, CPS can support two other parasitic modes (TE0 and TM_0) besides the fundamental CPS mode. Air-bridges are frequently employed in CPS to suppress the propagation of the parasitic modes. But the use of air-bridge will increase the fabrication difficulty due to the fact that microfluidic channel will be located on top of the electrodes. Thus, without including a purposely-designed CPW-CPS transition, the bandwidth of the CPS is limited.

2.2.2. Electromagnetic Simulation

Three-dimentional full-wave finite-element simulation is achieved with the use of well-established commercial software ANSYS HFSS v14/v15. CPW is one of the basic

structures that can be simulated by HFSS. Guidelines for setting up the HFSS simulation are discussed briefly as in this section.

Port is a 2D surface on which the appropriate RF excited can be defined as input and output. Wave port (compared to lump port) is selected in this simulation. A rule-of-thumb dimension of the wave port is defined [11] as follows, shown in Fig. 2.3. The port height should be at least 4 times the height of the substrate to include the substrate effect. The air section below and above the substrate should be also included in the port region. Note that normally we assume a semi-infinite substrate to simplify any calculation.

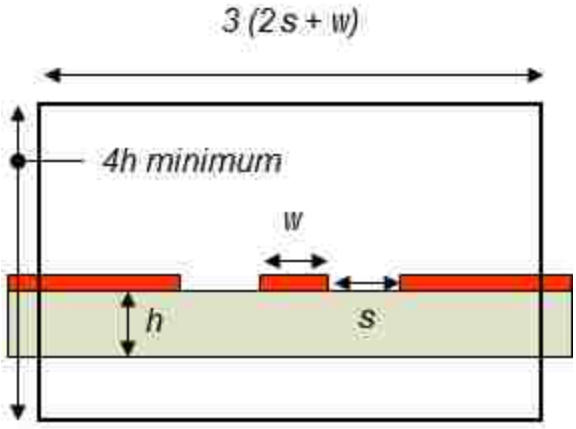

Fig. 2.3 General wave port setup of CPW in HFSS.

In this design, modifications are made in the simulation. Consider that the special CPW that we use has a fairly small gap of 10 um which is particularly chosen to be comparable to cell size, the electric field is more confined in the gap region of CPW with smaller radiation loss. Thus, a smaller port is implemented, as shown in Fig. 2.4 . The air box is used to define the solution area. The material outside the air box is set to perfect conductor by default. Radiation boundary condition on the air box is applied to insure that all the energy will be absorbed into the radiation boundary instead of being reflected back

to the simulated structure. The dimensions of the wave port and air box are well selected until no artificial effect introduced to the simulation by varying the parameters. Fig. 2.4 (a) and (b) show the electrical field concentrated at the gap of the CPW where the cells are mostly trapped. Adaptive mesh is applied in HFSS, as shown in Fig. 2.4 (c). HFSS could also provide the information of reflected and transmitted signal from the simulated structure, which are defined as Scattering (S) parameters and will be discussed in next section.

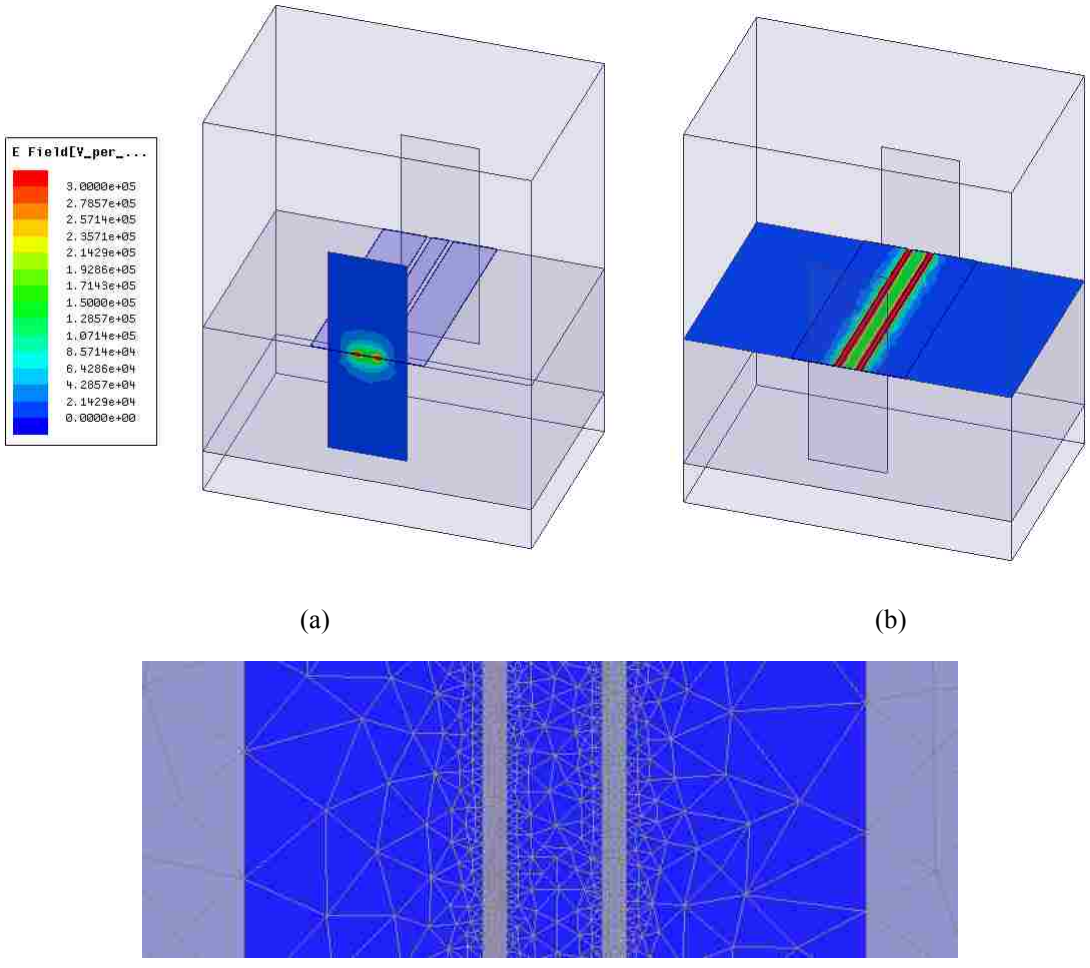

(a) (b)

(c)

Fig. 2.4 Electrical field distribution in coplanar waveguide structure with an input of 1W. (a) E-field at wave port. (b) E-field in x-y plane. (c) Adaptive mesh achieved by HFSS.

2.2.3. Scattering Parameters

S parameters, which are elements of a scattering matrix, represent reflection and transmission coefficients of the N-port network. Unlike the Z-parameters or Y-parameters, S-parameters are mostly used for networks operating at radio frequency where open or short circuit condition doesn't exist. Signal power is easily quantified than current and voltages at high frequency where the physical length of the transmission line is long compared to the wavelength of the signal.

As shown in Fig. 2.5, in the two-port network with incident wave a_1 and reflected wave b_1 at port 1 and incident wave a_2 and reflected wave b_2 at port 2, the S parameters can be defined as follow [12]:

$$\begin{bmatrix} b_1 \\ b_2 \end{bmatrix} = \begin{bmatrix} S_{11} & S_{12} \\ S_{21} & S_{22} \end{bmatrix} \begin{bmatrix} a_1 \\ a_2 \end{bmatrix} \tag{2.5}$$

where

$S_{11} = \left.\frac{b_1}{a_1}\right|_{a_2=0}$, input reflection coefficient with output properly terminated;

$S_{21} = \left.\frac{b_2}{a_1}\right|_{a_2=0}$, forward transmission coefficient with output properly terminated;

$S_{22} = \left.\frac{b_2}{a_2}\right|_{a_1=0}$, output reflection coefficient with input properly terminated;

$S_{12} = \left.\frac{b_1}{a_2}\right|_{a_1=0}$, reverse transmission coefficient with input properly terminated.

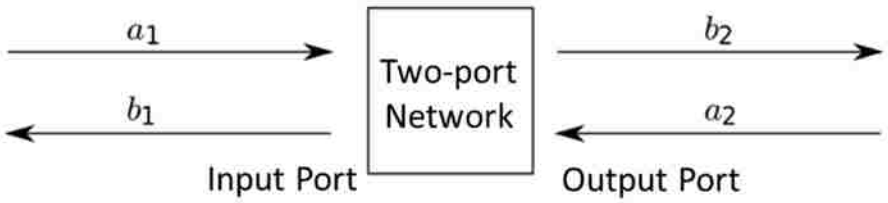

Fig. 2.5 Incident and reflected waves in a two-port network

Note that, S parameters vary with frequency; therefore, their values over frequency is usually measured by the electrical measurement equipment Vector Network Analyzer (VNA). Moreover, if a system is passive, the network is reciprocal where $S_{11} = S_{22}$ and $S_{21} = S_{12}$ will be observed.

Usually, the scalar logarithmic (decibel or dB) expression for S parameters is more commonly used than scalar linear expression. The insertion loss (IL) is the magnitude of the transmission coefficient $|S_{21}|$ expressed in decibel,

$$IL = -20\log_{10}|S_{21}| \text{ dB} \tag{2.6}$$

While the return loss (RL) is the magnitude of the reflection coefficient $|S_{11}|$ expressed in decibel,

$$RL = -20\log_{10}|S_{11}| \text{ dB} \tag{2.7}$$

In the following discussion, S parameters will be measured to characterize the system from its transmission and reflection signals in high frequency.

2.2.4. Detailed Design Parameters

There are two different electrode designs that need to be discussed: CPW on quartz and CPS on sapphire. Both of them have several design considerations in common: First

of all, they are both terminated with SMA connectors at the end, which establishing an easier connection to the measurement environment compared with wafer-probing. Secondly, the electrical parts of them are fabricated with external vendor, Applied Thin-Film Products, Fremont, CA. The waveguide is made of 2-um-thick gold deposited on a 635-um-thick substrate. The thickness of the gold material is selected for the lower loss performance in regular RF components like phase shifter [13]. The substrate height should be large enough for the assumption of semi-infinite ground substrate for CPW and also for the consideration of the mechanical strength. The height of 635 um is a compromise of mechanical property and limitation of the microscope's focus distance, and also within the options that were provided by vendor [14]. Thirdly, the gap between the signal line and ground line is designed to be 10 um, which is the smallest size that limited by vendor's fabrication capability. The choice of the biological cells is then also dependent on the gap width.

Considering an inverted microscope is used in the experiment, there are only two options for the substrate due to the requirement of transparency: quartz (SiO_2,) and sapphire (Al_2O_3, ϵ=9.8).

The design of CPW on quartz microscope slide [8] is presented in Fig. 2.6(a). The portion of the waveguide under the micro-channels has a wavy pattern to help trap the cells mechanically and concentrate the electric field locally as shown in Fig. 2.6 (b). The different wavy patterns and the 8 parallel channels are used to look for the most efficient traps for cells. However, it doesn't significantly improving the trapping performance. Thus in later design, only straight lines of CPW are used.

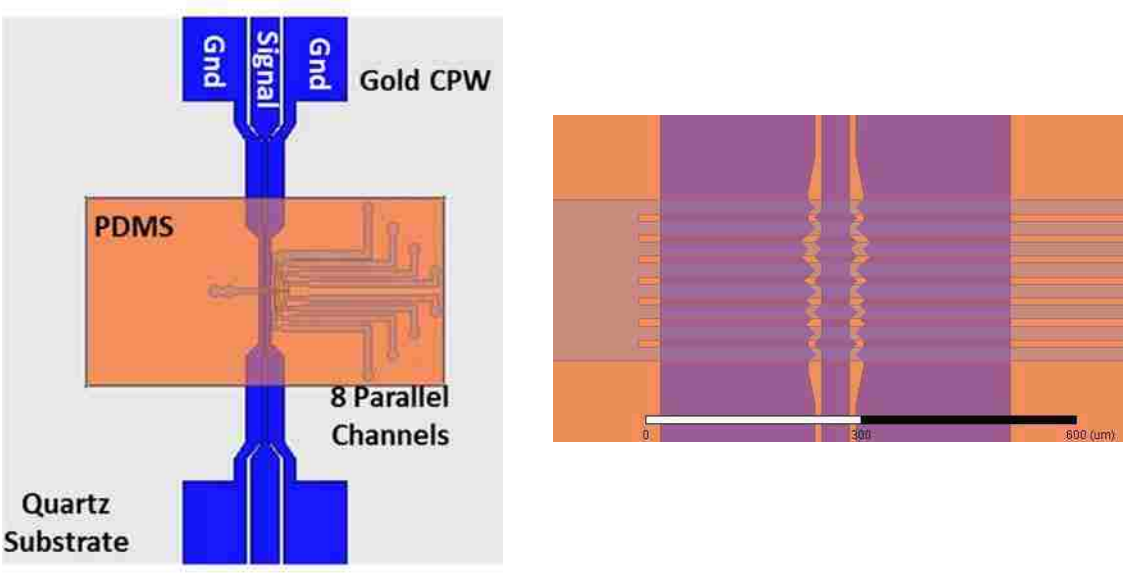

(a) (b)

Fig. 2.6 Schematic of the SMA-terminated test chip based on coplanar waveguide. (a) Top view of the entire chip. PDMS cap is represented in the orange color. (b) A zoom in of the wavy trap region.

An impedance match over a specific bandwidth is also needed in order to reach a large return loss and a small insertion loss. Normally, radio frequency (RF) system is built on a 50-ohm system. By well-designed the dimension of the CPW, a characteristic impedance (Z_0) close to 50ohm will be reached, which can be calculated from equation . After simulation and turning with HFSS, the design parameters are reported in Table 2.1. Photo of the fabricated devices are presented in Fig. 2.7.

Table 2.1 Design Parameters of SMA-terminated test chip based on coplanar waveguide

	Signal (um)	Gap (um)	Gnd (um)
1st step, SMA termination	1300	220	2800
2nd step, Transition	140	45	700
3rd step, Detection Region	40	10	220

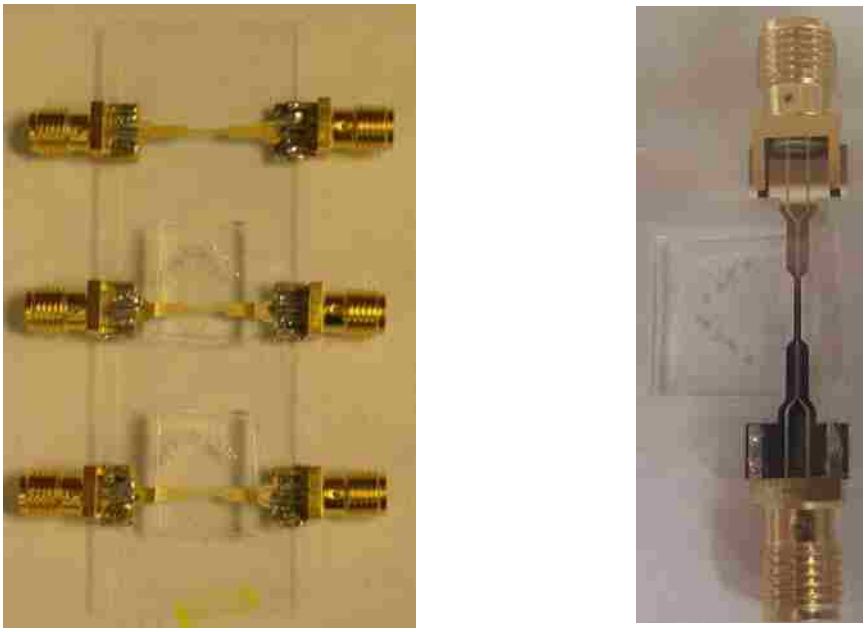

(a) (b)

Fig. 2.7 Photo of the assembled chip terminated with SMA connectors. (a) Top view (b) Bottom view

CPS on sapphire is also designed, fabricated and tested [15][16]. As discussed in Section 2.2.1, CPS has several advantages over CPW like small shunt parasitic capacitance and trapping cells in one slot other than two. Moreover, replacing quartz with sapphire offers additional advantages: Firstly, higher permittivity allows more compact electrodes with smaller gaps, higher electric field, and less optical obscurity. To obtain a CPS with a characteristic impedance of 50 ohm with a fixed gap of 10um, the electrodes are narrower with higher permittivity. Also, sapphire substrate provides better mechanical strength to prevent breakage especially when coaxial cables and fluid tubes are attached.

In addition, the dimension of PDMS cap is 0.5-mm in height and 1-mm in width, inside which the microfluidic channel is 50-um in height and 1-mm in width. The microfluidic channel has inlets and three outlets so that it could provide the steering control of the fluids to direct the cell flow. All the device parameters that chosen through

optimization using HFSS are summarized in Table 2.2. Schematic is reported in Fig. 2.8 (not in scale).

Fig. 2.10 shows that, up to 1GHz, there is little difference in the measured scattering parameters on a microchamber with the microfluidic channel filled with air or the sucrose buffer, or without the PDMS cover altogether. The measured scattering parameters are close to that simulated by using HFSS. In all case, the insertion loss is less than 1.5 dB for the transmitted signal S_{21} and the return loss is greater than 10 dB for the reflected signal S_{11} up to 2GHz. Below 1 GHz, the impedance match is best for the sucrose case as

Table 2.2 Design Parameters of SMA-terminated test chip based on coplanar stripline

	Signal (um)	Gap (um)	Gnd (um)
1st step, SMA termination	1300	600	2900
2nd step, Transition	600	60	600
3rd step, Detection Region	100	10	100

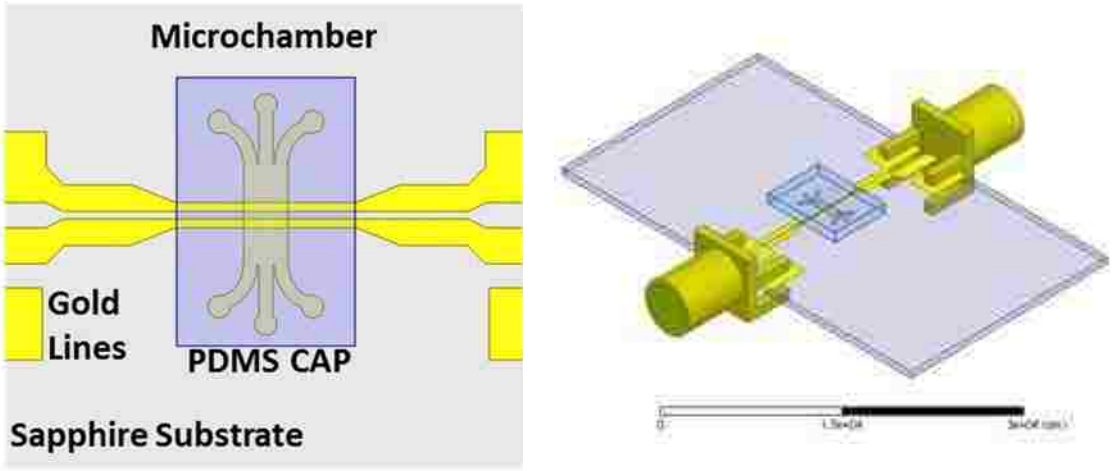

(a) (b)

Fig. 2.8 Schematic of the SMA-terminated test chip based on coplanar stripline (a) Top view (b) 3D view.

indicated by the lowest S_{11}. Above 1GHz, the shunt capacitance of the microfluidic channel degrades the impedance match of the coplanar stripline. The degradation effect is stronger on a CPS than on a CPW, resulting in a narrower bandwidth of the present microchamber than that of the previous CPW design.

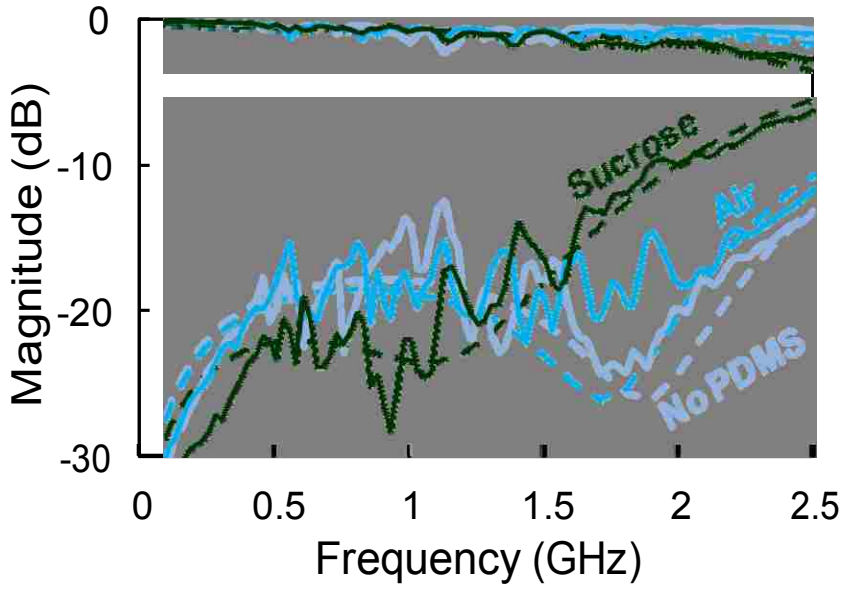

Fig. 2.9 Measured (solid curves) vs. simulated (dashed curves) transmission (S_{21}) and reflection (S_{11}) scattering parameters for the microchamber with its microfluidic channel filled with air or the sucrose buffer, or without the PDMS cover altogether.

2.3. Dielectrophoresis

Apart from the detection of the incident and reflected signal, another important part of the electrical measurement of the target biological cells is how to manipulate and separate the cells with the electrical signal. Over the past 10 years, the most widely-used and popular way of manipulation is dielectrophoresis (DEP), which is first introduced by Pohl[17]. The development of DEP mad contribution to the areas of biosensors, cell therapeutics, drug discovery, medical diagnostics, microfluidics, nanoassembly, and particle filtration [18]. DEP takes advantage of the non-uniform electric field that induces

the dipole moment and manipulates the cell. An example of DEP in separation of viable and non-viable yeast cells are presented in Fig. 2.10 [19].

The DEP force is determined by the size of the particle, gradient of the electric field, the permittivity difference of the particle and medium. Theoretically, the DEP force can be calculated by [20]

$$F_{DEP} = 2\pi r^3 \varepsilon_m \mathrm{Re}\left(\frac{\varepsilon_p^* - \varepsilon_m^*}{\varepsilon_p^* + 2\varepsilon_m^*}\right)\left(\nabla E^2\right) \tag{2.8}$$

with the Clausius-Mossotti factor equals to

$$CM = \left(\frac{\varepsilon_p^* - \varepsilon_m^*}{\varepsilon_p^* + 2\varepsilon_m^*}\right). \tag{2.9}$$

where r is the radius of a homogeneous sphere, ε_m and ε_p are the dielectric constant of the media and the particle respectively, and E represents the electric field. Positive or negative

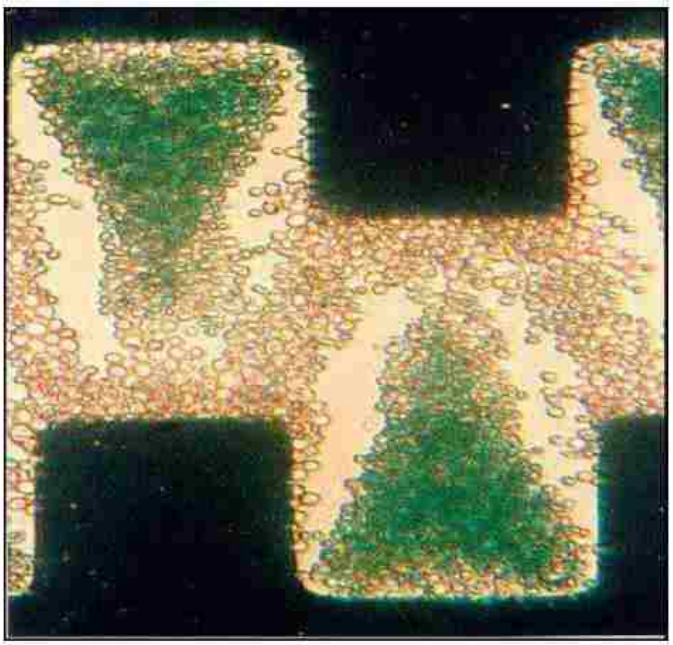

Fig. 2.10 Dielectrophoretic separation of viable and non-viable yeast cells using interdigitated, castellated electrode with a 10 MHz signal [19].

DEP force is decided by CM factor and it would lead the particle to the highest field region or lowest field region due to differences of the particle and media. To be specific, if a suspended particle has a polarizability higher than the medium, DEP force will push the particle towards the highest field region, which is a positive DEP. Vice versa, if a medium has a higher polarizability than the suspended particle, the particle is driven towards the lowest field region, which ends up with a negative DEP. From Fig. 2.11, we can tell that DEP mainly works at KHz – MHz range.

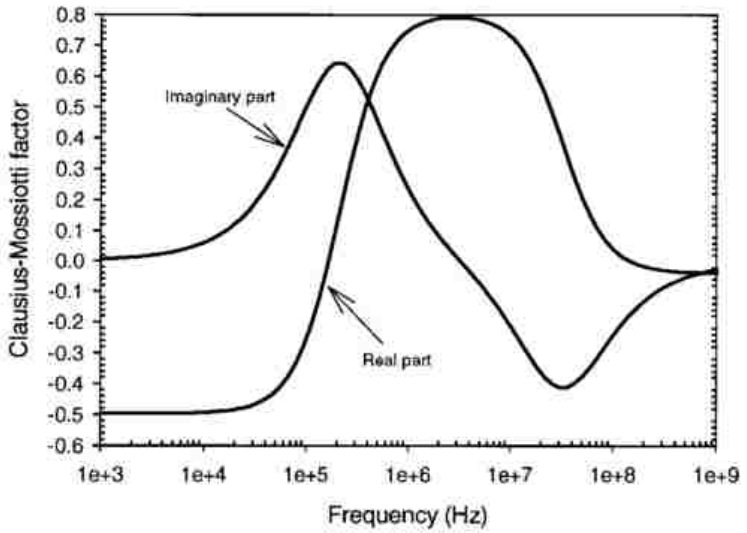

Fig. 2.11 A general plot of the Clausius-Mossiotti factor experienced by the cells when suspended in a medium [32].

Three-dimension full-wave simulation by HFSS has been done to study the electrical field and the gradient of the electric field along the CPW electrodes in the specific designs thus to confirm the trapping performance, as in Fig. 2.12. The energy that travels along the CPW is concentrated to the gap due to the CPW mode. The wave shape of the electrodes are used to further concentrate the electric field, and to provide a higher gradient of electric field, It also acts further as a mechanical trap that facilitates the cell trapping.

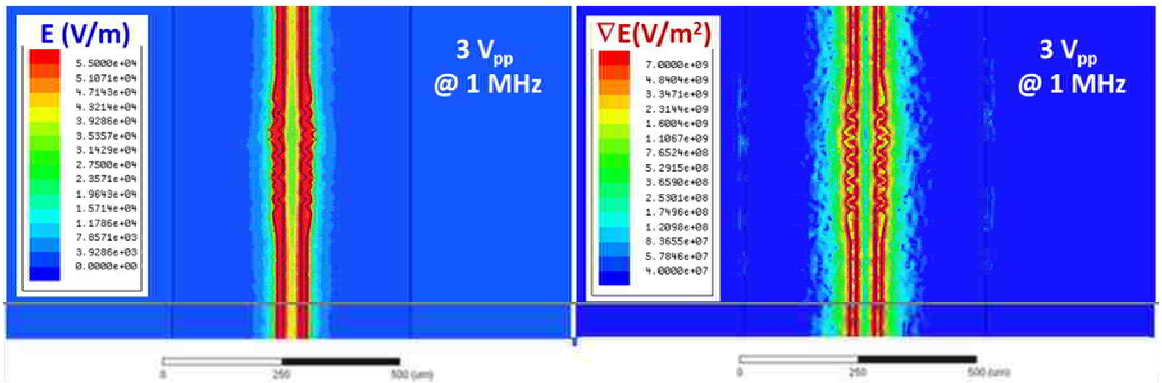

Fig. 2.12 HFSS simulation of the electric field (left) and the gradient of the electric field (right) of a coplanar waveguide structure.

2.4. Fabrication of Microfluidic Channel

Polydimethylsiloxane (PDMS) has many advantages in structural, chemical, physical aspects serving as the fabrication material for microfluidic channels. PDMS is transparent to begin with which allows optical detection. Electrically, PDMS has a breakdown voltage of 2×10^7V/m. It is impermeable to liquid water but permeable to gases and nonpolar organic solvent. The non-toxicity and biocompatibility makes it a perfect fit for biomedical applications [21][22][23].

The general fabrication process is shown in Fig. 2.13. Soft lithography and replica molding of microfluidic devices are first made. Then pour the liquid pre-polymer over the master and cure it. After peel the PDMS from the master mold, surface oxygen plasma is used to form an irreversible seal between PDMS and the substrate by generating silanol groups (Si-OH) on the surface of the contact. With the golden electrodes deposited on top

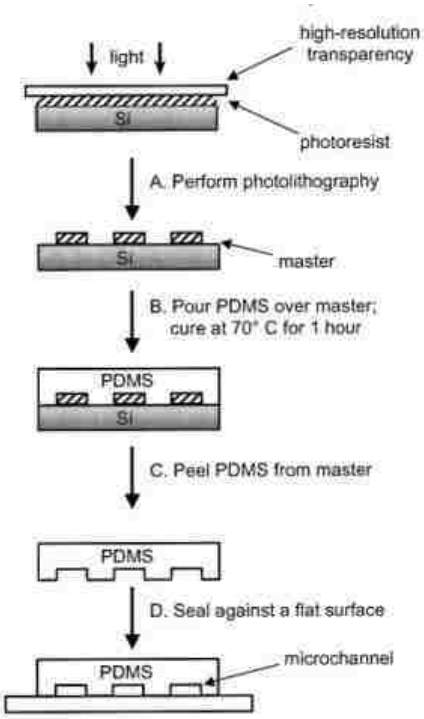

Fig. 2.13 Schematic of fabrication process of the microchannel [22].

of the substrate, the bonding of PDMS over the gold region is not fully sealed. To solve the problem, silica were painted close to the electrode for sealing purpose and mechanical holders are also used. The input and output of the microfluidic channel are opened with needles. After assembling the tubes, the microchamber is assembled and ready for testing.

2.5. Off-chip Cell Preparation

2.5.1. Cell Culture

To test the present electrode design, Jurkat (immortalized T-lymphocyte line) cells and HEK 293 (embryonic kidney) human cells were chosen for their robustness, large size (~7 μm for Jurkat cells and ~15 μm for HEK cells), and relatively simple structure, as in Fig. 2.14.

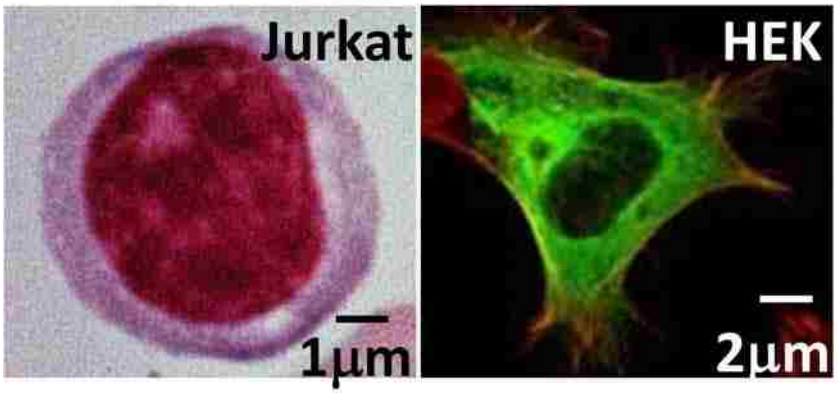

Fig. 2.14 Microscopy image of Jurkat (left) and HEK (right) cell.

The cell preparation process is summarized in Fig. 2.15. Jurkat cells are cultured under 5% CO_2 at 37ºC in a media based on Sigma-Aldrich's RPMI 1640 with 10% fetal bovine serum, 100 units/ml penicillin, and 100 μg/ml streptomycin. HEK cells were cultured in DMEM high glucose with 10% fetal bovine serum, 100 units/ml penicillin, and 100 μg/ml streptomycin. The cells are measured in the suspended state, after removal from culture plates with trypsin enzyme. The cultured Jurkat cells and HEK cells were washed

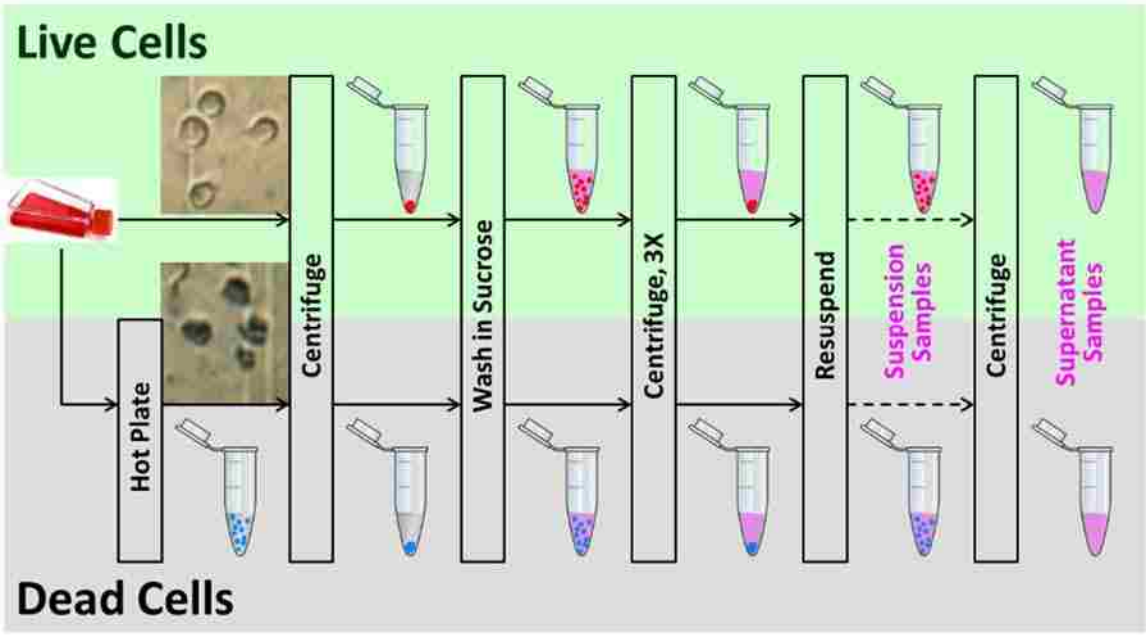

Fig. 2.15 Cell preparation process of live and dead cells.

with 8.5% sucrose plus 0.3% dextrose, then twice resuspended to a concentration of 3 $\times$ 10^6 cells/ml before injection through the microfluidic channel. The sucrose solution ensures cell viability while reducing parasitics such as solution conductivity and electrode polarization [24].

To check cell viability, trypan blue was used in a separate experiment to confirm that approximately half of the cells survived after 10 h, as shown in Fig. 2.16. Trypan blue is a dye that can be used to differentiate live or dead cells due to the fact that intact cell membranes will prevent the dye to go inside the cytoplasm while dead cells will take the dye and become blue color [25]. To deliberately kill the cells, separate suspensions of Jurkat cells in sucrose/dextrose solution were placed on a 115ºC hot plate for 6 min. Cell death was verified by trypan blue staining. Trypan blue was never used on cells that were subjected to electrical detection in order to keep the detection label free.

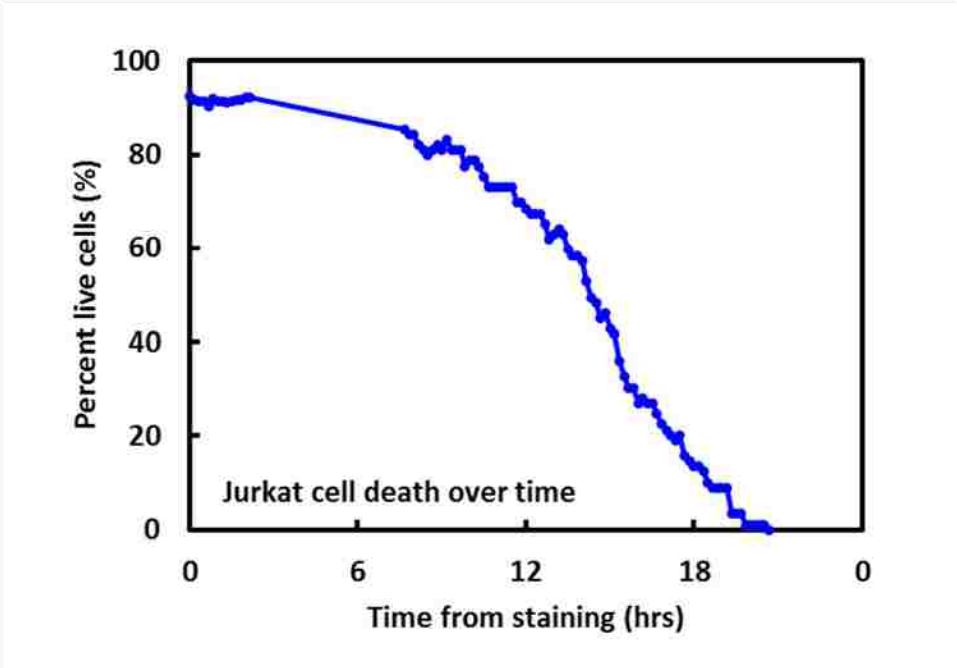

Fig. 2.16 Jurkat cell death over time in 8.5% sucrose/0.3% dextrose in microchannel - stained with trypan blue.

2.5.2. Media Selection

Considering the fact that biological cells cannot live without the solution environment, the volume of solution is much larger than the cell themselves even microfluidic channel is in use. Solution is still the most important factor to be understood before the detection of biological cells. Thus, it is necessary to study the effect of the media and select up the right solution due to the specialty of the biological cells. Here are more detailed explanations on why a suspended media of sucrose is selected for experiment.

Biological cells can stay alive in several medium options. First is the cell growth medium which provides everything cells need to live and multiply. However the difficulty is that its high conductivity brings the polarization effect, also it is hard to control due to cells' continuous activity. The second option could be phosphate buffered saline (PBS) which is also a high conductive solution; while the third option could be a sugar-based low conductive viability-maintenance solution containing 8.5% sucrose and 0.3% dextrose. The cells could not stand in DI water as cells suspended in DI water would lyse immediately [26].

High ionic solution will generate electrode polarization effect especially in low frequency range and the unwanted parasitic effect during a dielectric experiment will mask the dielectric response of the sample. As discussed by Schwan[27], the impedance of electrodes, which is in series with impedance of the suspension, adds increasingly to the measured impedance. As the frequency is decreasing, the accumulation of charges at the electrode-solution interface leads to an increase of both real and imaginary part of the dielectric constant of the targeted sample. Lots of study have been done on understanding

and eliminating the effect on electrode polarization [27][28][29][30]. One of the advantages of measuring in the GHz range is to reduce this effect, where the charges cannot catch up with the change of the signals.

Moreover, as stated in [31], 2-D electromagnetic simulation with COMSOL Multiphysics v. 4.3 is done to verify the current fluxes for a Jurkat cell that suspended in different media. Fig. 2.17 plots the distribution of the normalized current fluxes at 10ns in two possible media choice: (1) 8.5% Sucrose with σ_{extra}= 0.056 S/m, and (2) 1X PBS with σ_{extra} = 0.55 S/m. And the cytoplasm conductivity of Jurkat cells is simulated to be σ_c= 0.32 S/m [31]. From these results, we can tell that the low conductivity media will force most sensing current through cytoplasm, and it is better to be applied in the experiment.

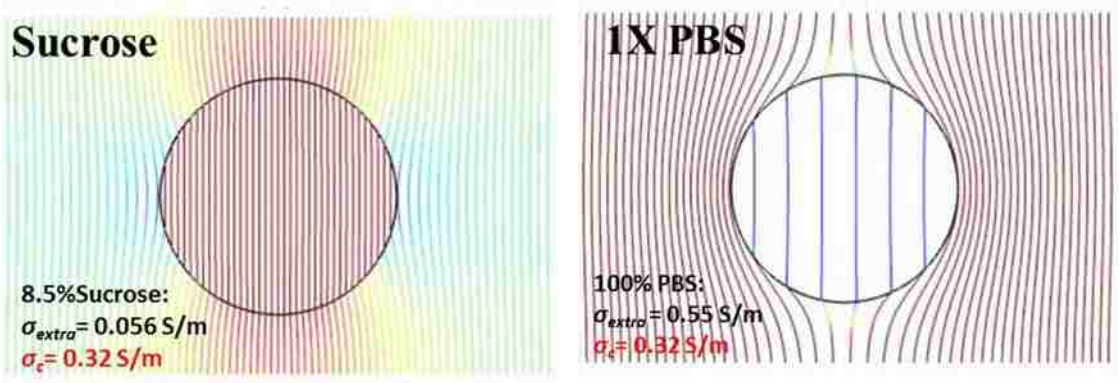

(a) (b)

Fig. 2.17 Simulated current fluxes for a Jurkat cell suspended in (a) 8.5% sucrose and (b) 10X PBS between two 20-um wide electrodes 10-um apart [31].

In addition, electrolysis was unexpectedly observed in the medium of 0.1X PBS at low voltage, which results in a broken gold electrodes, as shown in Fig. 2.18. The test of the 8-channels chip is to find out where is the hot spot for trapping the cells since different trapping structure is used. However, it suffers from severe clogging issue because the channel width is only 20um and debris of the cells easily get jammed. Later after this series

of exploration, a large channel of 150um is fixed to be used in the experiment. We trade off the electric impedance match to the smooth flow in the microfluidic system.

Fig. 2.18 (a) shows the device with 8 parallel channels filled with Jurkat cells in PBS solution. After turning on the DEP signal, a significantly increase in electrolysis of gold was found, as shown in Fig. 2.18 (b). Sucrose solution was not observed similar issue.

Due to above-mentioned reasons, the cells are chose to resuspended in the medium of sucrose instead of PBS for further study.

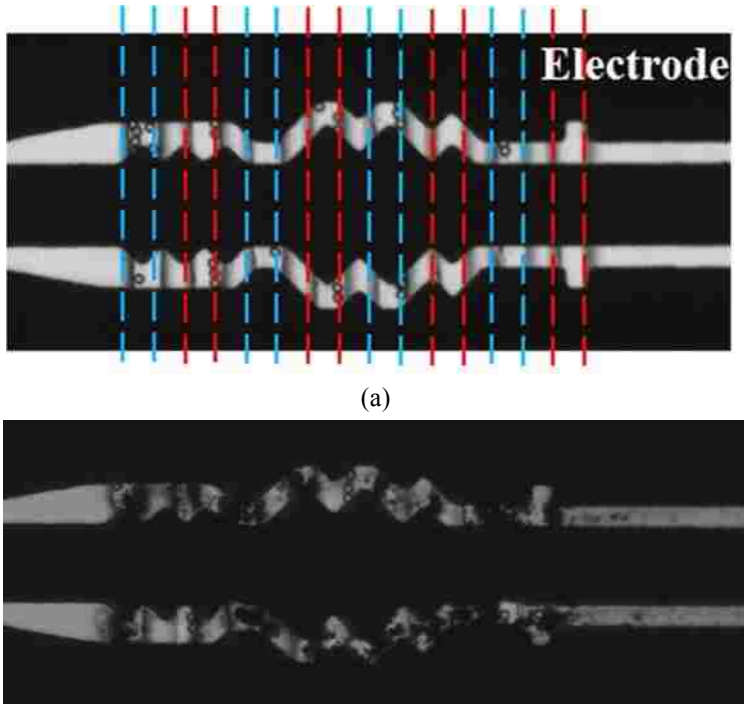

(a)

(b)

Fig. 2.18 .Electrolysis in PBS solution with gold electrode at low voltage. (a) Before having the DEP signal with cell trapped in the 8 parallel channels configuration. (b) After the DEP signal, there is a considerably ruin of the gold electrodes.

2.6. Frequency Dependent Dielectric Property

The dielectric property of the solution is significantly important in terms of a bio-related design in which solution plays a significant role in the measurement. As mentioned

in previous section, with the permittivity decreasing as the frequency increases, the characteristic impedance of the CPW line also varies. Thus a Keysight (Agilent) 85070E 500 MHz–26.5 GHz Performance Probe was used for broadband characterization of the solution permittivity, as shown in Fig. 2.19. It can provide useful information about the materials to assist the design process of the device.

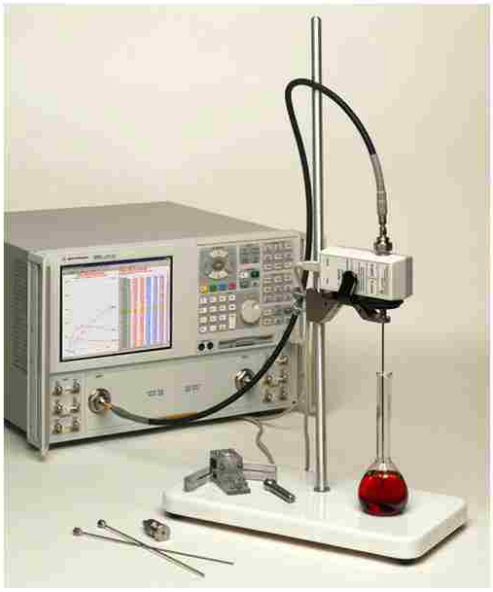

Fig. 2.19 Keysight (Agilent) 85070E Dielectric Probe together with Ecal used for precise characterization of the solution under test.

The complex permittivity measured by the probe as a function of frequency, as plotted in Fig. 2.20 was then used in conjunction with the dimensions of the CPW, PDMS and channel in the HFSS simulation of S parameters shown in Fig. 2.21. Due to the consideration of the frequency-dependent permittivity which influences the character impedance of CPW thus lead to the matching condition, as well as the frequency-dependent loss tangent which relates to the insertion, the HFSS simulation can fully estimate the matching and loss condition of the interested structure.

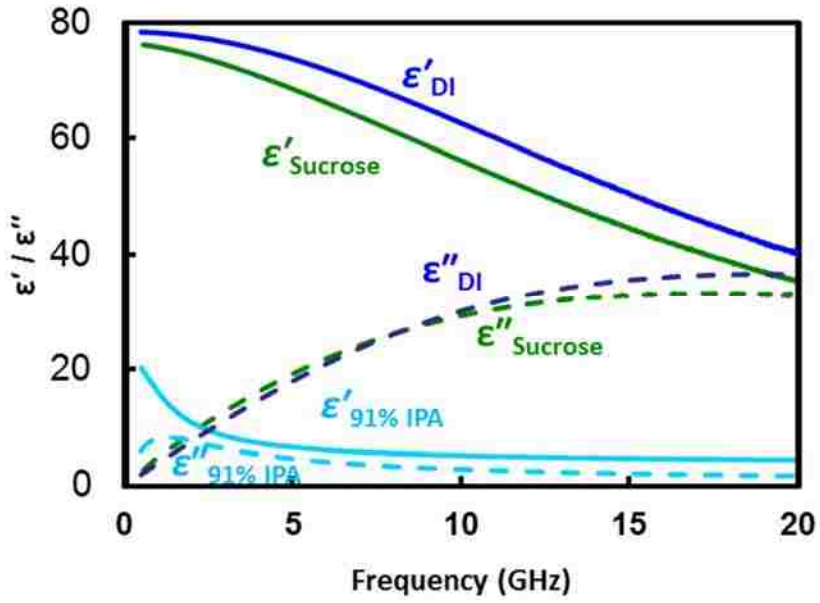

Fig. 2.20 Complex permittivity of DI water, sucrose and 91% IPA measured by Agilent 85070E

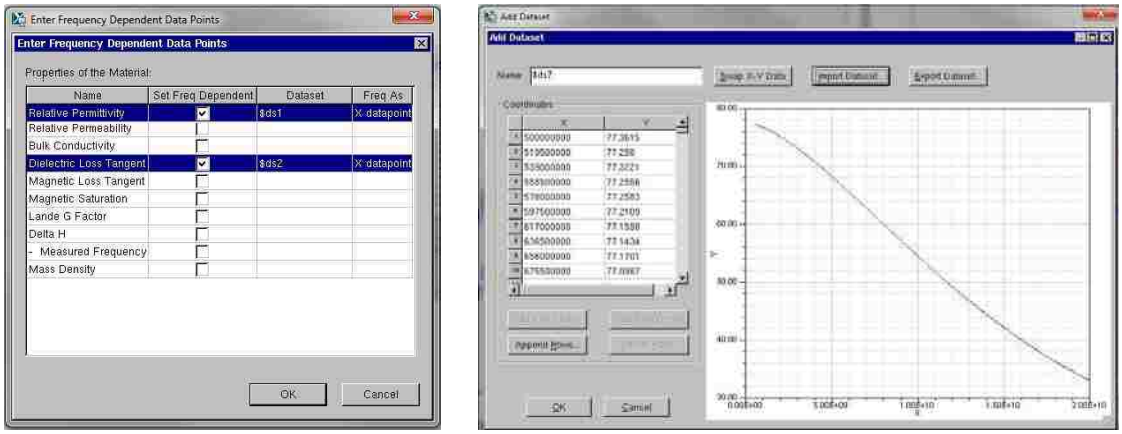

(a) (b)

Fig. 2.21 Frequency-dependent dielectric property set in HFSS simulation.

The effect of the including the freq-dependent dielectric property is confirmed with on-wafer CPW which has a designed gap / signal / gap value of 10 um / 40 um / 10um on quartz substrate. It has a characteristic impedance of 58 Ω without the PDMS and 51 Ω with the PDMS cover in which microchannel is filled the air. With the microfluidic channel filled with aqueous solutions, the CPW capacitance increases and the characteristic

impedance decreases generally. Meanwhile, the CPW becomes more dispersive below the solution and the characteristic impedance becomes more sensitive to the length and thickness of the CPW, PDMS, and channel. For example, with the solution permittivity varying from 78 to 35, as in Fig. 2.20, between 500 MHz and 20 GHz, the characteristic impedance varies between 12 Ω and 18 Ω. Thus, for broadband electrical detection to elucidate the dispersive characteristics of biological cells, the dispersive characteristics of the test chip need to be calibrated first.

References

[1] C. P. Wen, "Coplanar Waveguide: A Surface Strip Transmission Line Suitable for Nonreciprocal Gyromagnetic Device Applications," IEEE Trans. Microw. Theory Tech., vol. 17, no. 12, pp. 1087–1090, Dec. 1969.

[2] R. N. Simons, Coplanar Waveguide Circuits, Components, and Systems. John Wiley & Sons, 2004.

[3] A. Raj, W. S. Holmes, and S. R. Judah, "Wide bandwidth measurement of complex permittivity of liquids using coplanar lines," IEEE Trans. Instrum. Meas., vol. 50, no. 4, pp. 905–909, 2001.

[4] J.-M. Kim, D. H. Oh, J.-H. Park, J.-W. Cho, Y. Kwon, C. Cheon, and Y.-K. Kim, "Permittivity measurements up to 30 GHz using micromachined probe," J. Micromechanics Microengineering, vol. 15, no. 3, pp. 543–550, Mar. 2005.

[5] J. C. Booth, N. D. Orloff, J. Mateu, M. Janezic, M. Rinehart, and J. A. Beall, "Quantitative Permittivity Measurements of Nanoliter Liquid Volumes in Microfluidic Channels to 40 GHz," IEEE Trans. Instrum. Meas., vol. 59, no. 12, pp. 3279–3288, Dec. 2010.

[6] S. Seo, T. Stintzing, and I. Block, "High frequency wideband permittivity measurements of biological substances using coplanar waveguides and application to cell suspensions," … Dig. 2008 IEEE …, pp. 915–918, 2008.

[7] K. Grenier, D. Dubuc, P.-E. Poleni, M. Kumemura, H. Toshiyoshi, T. Fujii, and H. Fujita, "Integrated Broadband Microwave and Microfluidic Sensor Dedicated to Bioengineering," IEEE Trans. Microw. Theory Tech., vol. 57, no. 12, pp. 3246–3253, Dec. 2009.

[8] C. Palego, C. Merla, Y. Ning, C. R. Multari, X. Cheng, D. G. Molinero, G. Ding, X. Luo, and J. C. M. Hwang, "Broadband microchamber for electrical detection of live and dead biological cells," in 2013 IEEE MTT-S International Microwave Symposium Digest, 2013, pp. 1–3.

[9] T. Chen, F. Artis, D. Dubuc, J. J. Fournié, M. Poupot, and K. Grenier, "Microwave biosensor dedicated to the dielectric spectroscopy of a single alive biological cell in its culture medium," in IEEE MTT-S International Microwave Symposium Digest, 2013, pp. 1–4.

[10] G. Voskerician, M. S. Shive, R. S. Shawgo, H. von Recum, J. M. Anderson, M. J. Cima, and R. Langer, "Biocompatibility and biofouling of MEMS drug delivery devices.," Biomaterials, vol. 24, no. 11, pp. 1959–67, May 2003.

[11] "ANSOFT HFSS v8 Training. Port Tutorial Series: Coplanar Waveguide (CPW)." .

[12] G. Gonzalez, Microwave Transistor Amplifiers: Analysis and Design, 2nd Editio. Prentice Hall, 1997.

[13] C. Palego, Zhen Peng, J. Hwang, D. Scarbrough, D. I. Forehand, and C. L. Goldsmith, "Compact Ka-band phase shifters using MEMS capacitive switches," in Microwave Integrated Circuits Conference, 2009. EuMIC 2009. European, 2009, pp. 511–514.

[14] "ATP - Substrate Types and Specifications." [Online]. Available: http://www.thinfilm.com/substrates.html.

[15] Yaqing Ning, C. Multari, Xi Luo, C. Palego, D. Molinero, Xuanhong Cheng, J. C. M. Hwang, and C. Merla, "Coplanar stripline microchamber for electrical detection of live and dead biological cells," in Proc. Euporpean Microwave Conference, 2013, pp. 475–478.

[16] Y. Ning, C. Multari, X. Luo, C. Palego, X. Cheng, J. C. M. Hwang, A. Denzi, C. Merla, F. Apollonio, and M. Liberti, "Broadband Electrical Detection of Individual Biological Cells," IEEE Trans. Microw. Theory Tech., vol. 62, no. 9, pp. 1905–1911, Sep. 2014.

[17] H. A. Pohl, “The Motion and Precipitation of Suspensoids in Divergent Electric Fields,” J. Appl. Phys., vol. 22, no. 7, p. 869, Apr. 1951.

[18] R. Pethig, “Review article-dielectrophoresis: status of the theory, technology, and applications.,” Biomicrofluidics, vol. 4, no. 2, p. 022811, Jan. 2010.

[19] G. H. Markx, M. S. Talary, and R. Pethig, “Separation of viable and non-viable yeast using dielectrophoresis,” J. Biotechnol., vol. 32, no. 1, pp. 29–37, Jan. 1994.

[20] S. A. S. Wanjun Wang, Bio-MEMS: Technologies and Applications. 2006.

[21] J. C. Mcdonald, D. C. Duffy, J. R. Anderson, and D. T. Chiu, “Fabrication of microfluidic systems in poly (dimethylsiloxane),” Electrophoresis, vol. 21, pp. 27–40, 2000.

[22] J. C. McDonald and G. M. Whitesides, “Poly(dimethylsiloxane) as a Material for Fabricating Microfluidic Devices,” Acc. Chem. Res., vol. 35, no. 7, pp. 491–499, Jul. 2002.

[23] S. K. Sia and G. M. Whitesides, “Microfluidic devices fabricated in poly(dimethylsiloxane) for biological studies,” Electrophoresis, vol. 24, no. 21, pp. 3563–76, Nov. 2003.

[24] C. Cheng-Hsin, W. Ching-Hua, H. You-Ming, C. Hsiang-Ching, and W. Chin-Hung, “Depth effects of DEP chip with mierocavities array on impedance measurement for live and dead cells,” 3rd IEEE Int. Conf. Nano/Micro Eng. Mol. Syst. NEMS, pp. 858–863, 2008.

[25] W. Strober, “Trypan blue exclusion test of cell viability.,” Curr. Protoc. Immunol., vol. Appendix 3, p. Appendix 3B, May 2001.

[26] X. Cheng, Y. Liu, D. Irimia, U. Demirci, L. Yang, L. Zamir, W. R. Rodríguez, M. Toner, and R. Bashir, “Cell detection and counting through cell lysate impedance spectroscopy in microfluidic devices.,” Lab Chip, vol. 7, no. 6, pp. 746–55, Jun. 2007.

[27] H. P. Schwan, “Electrode polarization impedance and measurements in biological materials,” Ann. New York Acad. Sci., vol. 148, no. A1, pp. 191–209, Feb. 1968.

[28] H. P. Schwan, “Linear and nonlinear electrode polarization and biological materials,” Ann. Biomed. Eng., vol. 20, no. 3, pp. 269–288, Jan. 1992.

[29] F. Bordi, C. Cametti, and T. Gili, “Reduction of the contribution of electrode polarization effects in the radiowave dielectric measurements of highly conductive

biological cell suspensions.," Bioelectrochemistry, vol. 54, no. 1, pp. 53–61, Aug. 2001.

[30] P. Ben Ishai, M. S. Talary, A. Caduff, E. Levy, and Y. Feldman, "Electrode polarization in dielectric measurements: a review," Meas. Sci. Technol., vol. 24, no. 10, p. 102001, Oct. 2013.

[31] A. Denzi, C. Merla, C. Palego, S. Member, A. Paffi, Y. Ning, S. Member, C. R. Multari, X. Cheng, F. Apollonio, J. C. M. Hwang, L. Fellow, and M. Liberti, "Assessment of Cytoplasm Conductivity by Nanosecond Pulsed Electric Fields," IEEE Trans. Biomed. Eng., vol. 99, pp. 1–10, 2015.

[32] S. Archer, T. T. Li, a T. Evans, S. T. Britland, and H. Morgan, "Cell reactions to dielectrophoretic manipulation," Biochem. Biophys. Res. Commun., vol. 257, no. 3, pp. 687–698, 1999.

Chapter 3. Low Frequency and Time Domain Detection

3.1. Introduction

In Chapter 2, design considerations origin from both electrical side and microfluidics side were discussed. This chapter presents the system setup for both cases: low frequency (MHz) and time domain measurement.

In Chapter 3.2, a detection in the low frequency range of 100 Hz and 100 MHz has been done by using a precision impedance analyzer. The extracted shunt capacitance exhibits the well-known dispersion with increasing capacitance below 100 KHz and cut off above 1 MHz. In Chapter 3.3, measurements in time domain is reported, where nanosecond pulse is used without electroplating the cells. Results show that three reflection peaks associated with rise and fall of the incident bipolar pulse can be clearly delineated from the solution with trapped live cells, while the reflections from the one with dead cells are buried in background noise. Other experimental considerations are then discussed in Chapter 3.4, including the drift effect and cell viability. The early detection are achieved for understanding of the biological cells and prepare for the broadband detection.

3.2. Low Frequency Range Test

Many researchers have been focus on the lower frequency range of hundred Hz to MHz for the capacitance of the cell membrane and resistance of the cytoplasm with Keysight (Agilent) Impedance Analyzer / LCR meter [1][2][3][4]. We started in similar way of impedance spectroscopy to verify the system setup. The selected device is the coplanar stripline on sapphire terminated by SMA connector, which has been discussed in Section 2.2.

Fig. 3.1 (a) shows the microchamber under test on top of an inverted microscope. Fig. 3.1 (b) shows schematically the symmetric signal and ground electrodes of the coplanar stripline, which is narrowed down in the middle. The electrodes are made of 2-μm-thick gold deposited on a 635-μm-thick sapphire microscope slide with relative permittivity $\varepsilon_R = 9.3$. In the narrowed section, the electrodes are 100-μm wide and 10-μm apart.

With the microfluidic channel filled with the sucrose buffer containing Jurkat cells, the microchamber impedance was measured between 100 Hz and 100 MHz by using a

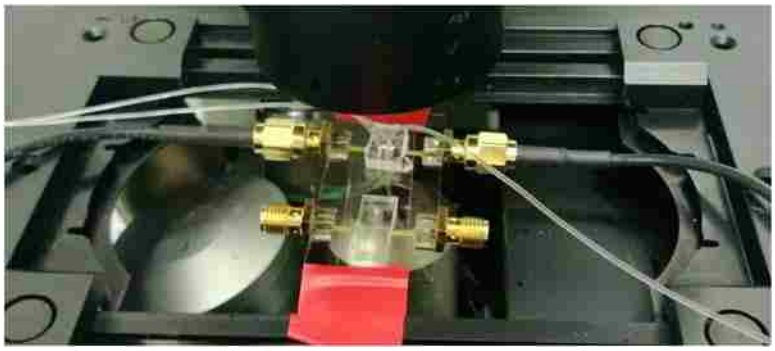

(a)

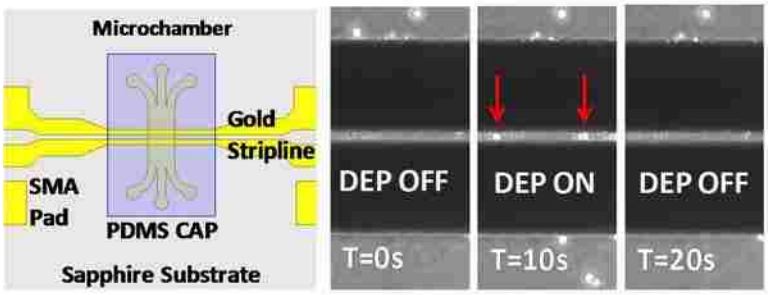

(b)

Fig. 3.1 (a) Improved microchamber under test on top of an inverted microscope. (b) Schematic of a coplanar stripline, which is narrowed down in the middle and intersected by a microfluidic channel at a right angle. (c) Two live cells trapped between the electrodes of the coplanar stripline 10 s after a dielectrophoresis signal is applied.

system setup found in Fig. 3.2. Keysight (Agilent) 4294A Precision Impedance Analyzer, 40Hz–110MHz, together with Keysight (Agilent) 16047A Text Fixture are used in the

measurement. Calibration is done with Agilent 3.5mm 85020D Calibration Kit, within a frequency range of 100Hz – 100MHz and the total number of points is 401. One port measurement is taken and the magnitude and phase of the impedances are recorded.

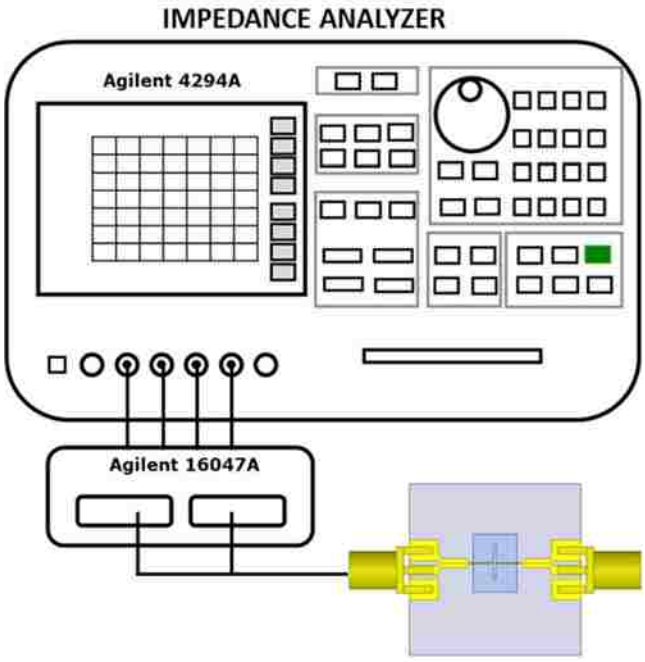

Fig. 3.2 Frequency domain experimental setup with Impedance Analyzer.

Fig. 3.3 (a) and Fig. 3.3 (b) show the frequency dependence of the magnitude and phase, respectively, of the measured impedance with several live or dead cells trapped. The data can be fitted reasonably well with a simple equivalent-circuit model shown in Fig. 3.4, which is sufficient to de-embed the intrinsic cell properties from the solution and electrode effects. De-embedding from the electrode effect is aided by comparing data measured by using the present coplanar stripline design and the previous coplanar waveguide design; de-embedding from the solution effect is aided by comparing data measured from cell

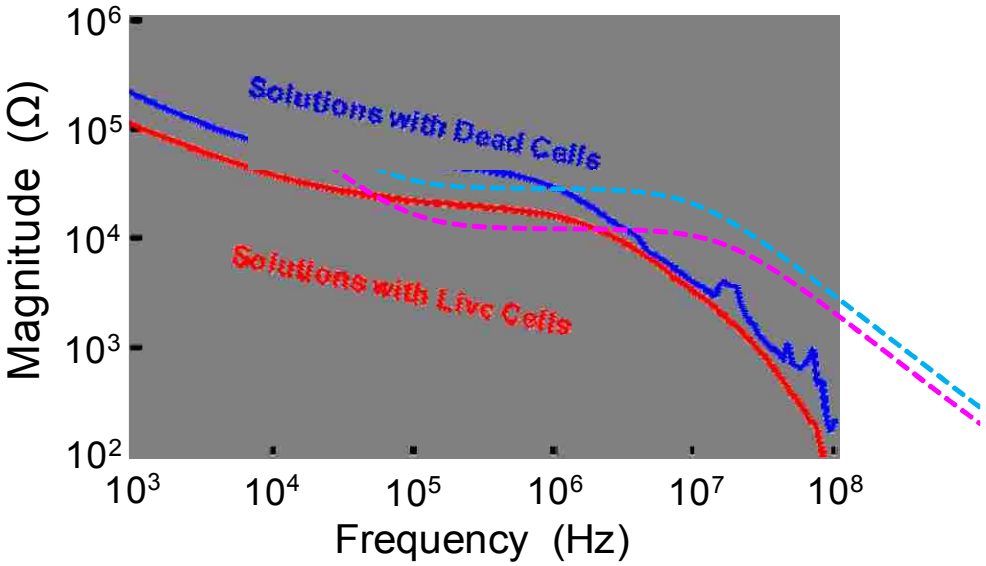

(a)

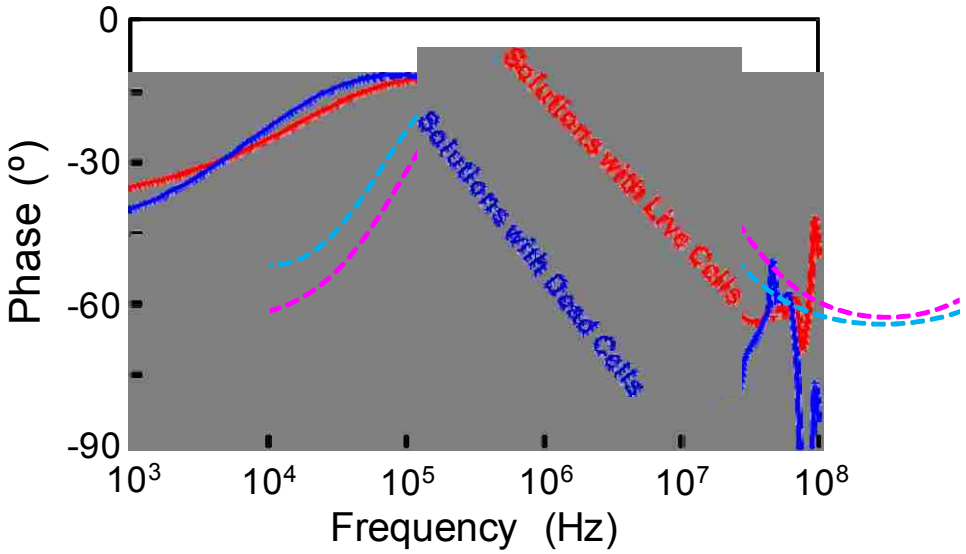

(b)

Fig. 3.3 Measured frequency dependence of impedance (a) magnitude and (b) phase with several live or dead cells trapped. Data (——) are fitted (- - -) with a simple equivalent-circuit model.

solutions and supernatant solutions. The resulting model parameters are listed in Table 3.1. Z_0, θ_0 and R_0 represent the characteristic impedance, electric length, and resistive loss, respectively, of the coplanar stripline. C_D accounts for electrode polarization. R_E and C_E

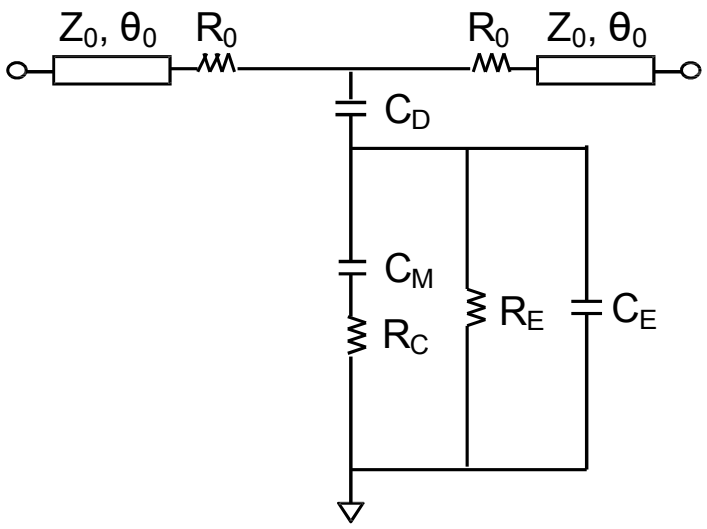

Fig. 3.4 Equivalent-circuit model

account for the solution effect. Finally, C_M and R_C model the cell membrane capacitance and cytoplasm resistance, respectively. The simplified electrical circuit analogue was first developed by Foster and Schwan [5] where cytoplasm in series with a capacitor for the membrane and then in parallel with the property of the suspending medium. The deviation between the measured and modeled phase response below 10 kHz is due to additional parasitic effects [6][7][8] not included in the present model.

It can be seen in Fig. 3.3 (a) that, consistent with the previous result obtained by using a coplanar waveguide[9], both the measured and modeled impedances exhibit the well-known dispersion with a flat band between 10 kHz and 1 MHz, where the difference between live and dead cells is the most prominent. As listed in Table 3.1, C_M is consistently higher for live cells, which reflects membrane integrity. On the other hand, R_C is consistently lower for live cells, which contradicts the trend observed in [10][11][12]. We believe the apparent contradiction is mainly due to the solution effect. In previous researches, thousands of cells in a solution are measured simultaneously and, as cells die,

Table 3.1 Model Parameters for Live and Dead Cells

Component	Parameter	Live/Dead
Stripline	$Z_0[\Omega]$	58
	$\theta_0[°]$	40 @1GHz
	$R_0[\Omega]$	12
Solution	C_D [nF]	1.2
	$R_E[k\Omega]$	300
	C_E[pF]	1.5/1
Cytoplasm	$R_C[k\Omega]$	20/49
Membrane	C_M[nF]	3.8/1

their membranes disintegrate and ions leak out to the surrounding solution to make it more conductive. In the present case, the ions that leak out of dead cells have been washed away before measurement and the measured result reflects better the intrinsic properties of cells, whose cytoplasm resistance is higher because fewer ions remain inside the cells. Presently, it is speculated that dead cells are larger than live cells with more solution displaced, which should increase, rather than decrease, the overall resistance [9].

3.3. Time Domain Study

In addition to the quantitative difference in impedance measured in the frequency domain, the nanosecond pulse that imposed onto the biological cells without electroporation can provide qualitative difference on the cell electrical. Especially, nanosecond pulse can be considered as a summation of high frequency signals in frequency domain.

Time-domain measurements utilizes a ±1.5-V 20-ns pulses with 2-ns rise/fall times and 2% duty cycle, generated by Keysight (Agilent 8110A) pulse generator. The pulse

signal also serves as the DEP signal to trap the cells. Bipolar signal minimizes electrode polarization, while short pulse and low duty cycle minimize cell heating. The final signals are examined by Keysight (Agilent) 86100A Infiniium Wide-Bandwidth Oscilloscope with Keysight (Agilent) 83484A two channel 50GHz Module. The system setup is a 2-port configuration shown in Fig. 3.5. The pulse signal first pass a power divider. One branch is connected directly into channel 1 of the oscilloscope which includes the information from the reflected signals. The other branch passes by the chip-under-test and then is sent to channel 2 of the oscilloscope which shows as the transmitted signals. By subtracting the

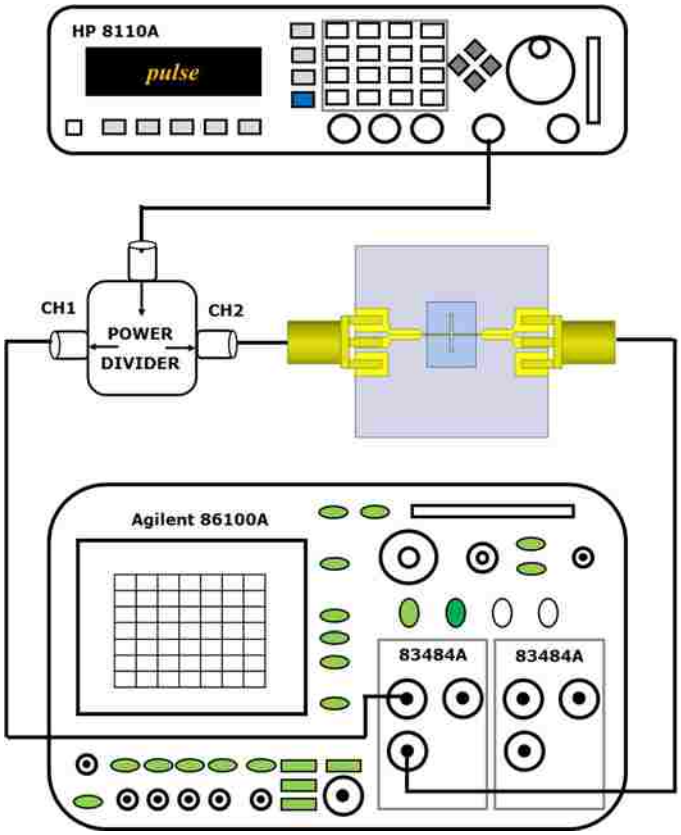

Fig. 3.5 Time domain experimental setup.

signal with live/dead cells from the signal without cells, the performance of the cell can be retrieved.

Fig. 3.6 shows the incident pulse signal and reflected signals from solutions with two trapped live and dead cells, respectively. In each case, reflection peaks associated with

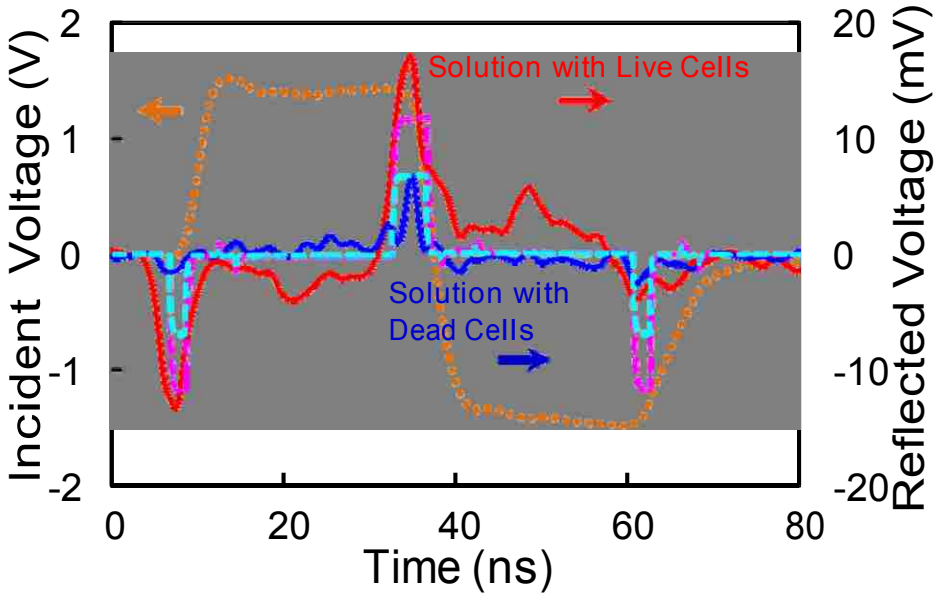

Fig. 3.6 Incident (dotted curve), measured reflection (solid curves), and simulated reflection (dashed curves) signals from solutions with two trapped live and dead cells, respectively.

the three rising and falling edges of the incident signal can be delineated. The measured reflections agree well with that modeled by using the equivalent circuit of Fig. 3.4. With a characteristic frequency on the order of 100 MHz, the reflections are mainly due to the shunt capacitance of the cell membrane. For the solution with trapped live cells, the reflections are consistently higher due to the higher capacitance of their intact membranes. Minor reflection peaks are not simulated by the present model, probably due to its over simplification.

Under a relatively long (~100 ns) pulse, most of the interaction between the pulse and the cell is across the cell membrane and the intracellular structure is shielded by the limited membrane capacitance. A nanosecond short pulse will expose the cell interior to the pulse by shorting out the membrane capacitance. With a current use of a 20ns-wide pulse with a rise and fall time to be both 2ns, a peak value of 2.9V is nevertheless insufficient for membrane poration. Simulations for different pulse amplitudes show that approximately 100 kV/cm would be required for a single nanopulse to induce poration almost instantaneously.

3.4. Experimental Considerations

As we go through the frequency domain measurement with impedance analyzer and the time domain study with the nanosecond pulse, we also gradually reshape our prototype measurement setup. Here are a couple of considerations that need to be paid attention to in the future.

3.4.1. Drift

During measurements for S parameters when the chip bonded with PDMS and channel filled with sucrose solution, a drift in both S_{11} and S_{21} is originally observed within a period of time when the solution is first injected into the microfluidic channel. As shown in Fig. 3.7, the signal is not stable until more than 20-min measurement. There are several potential reasons for the drifting: (1) The initial speed of the injected fluid into the channel is too fast. It always takes several minutes before the solution with a steady velocity. (2) There are ions leaching out from the PDMS. Since the sugar-based medium has a low conductivity, even if a small portion of leaked ions will have some impact. In the

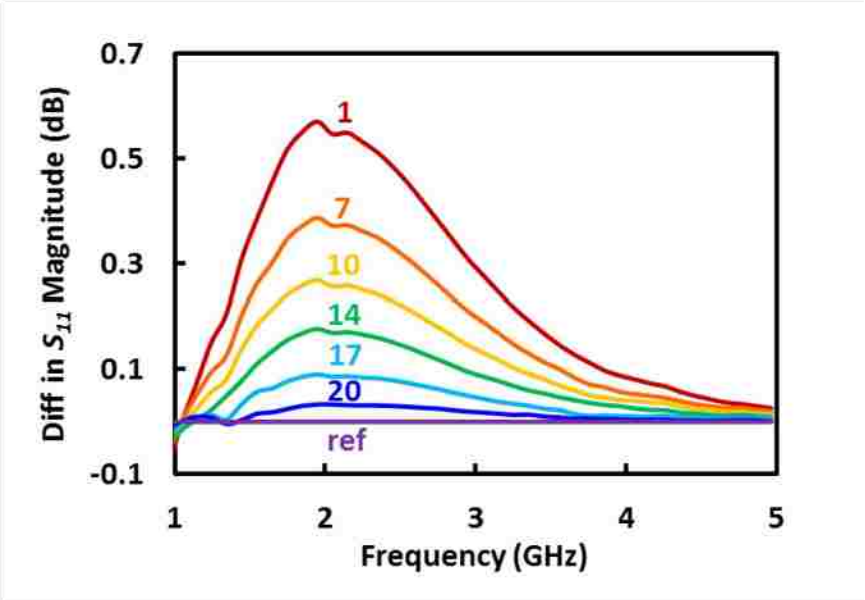

Fig. 3.7 Drift in the magnitude of S_{11} 0, 7, 10, 14, 17, 20 min after calibration without any cell trapped.

comparison experiment, the 10% PBS has shorter time to reach the stable condition. (3) The equilibrium of the temperature inside the microchannel might also have some influence.

To resolve above-mentioned assumption, actions have been made to reduce the drift problem. First, adjust the initial injection of the solution from syringe pump to be similar or at most 10 times faster than the cell trapping speed of 0.05 – 0.1 ul/min. Secondly, pre-soak the PDMS in DI water to wash away potential ions that stick to the channel wall. In the meanwhile, we reduce the IF band width to 5 Hz to further improve the stability of the electrical measurement as a trade-off of measurement speed of 3min/sweep. Biologically, we would like to have an instant measurement of the trapped cells without affecting the cell origin conditions. It also can be easy to control the number of trapped cells since there will be no cells that accidentally flow by the trapping region during the long sweep of the

entire bandwidth. However, electrically, average function or a narrow IF band width have to be used for low noise.

A new measurement protocol is also developed and mentioned in [13]. After a measurement is performed with 1 to 20 cells trapped, the DEP signal is turned off to allow the trapped cells to be washed away, and the measurement is repeated without any cell trapped as a reference. So that the difference between the two consecutive measurements can be regarded as the net effect of the trapped cells even if the calibration drifts with time. This is critical because, although the calibration does not drift by more than 0.01 dB per hour as in Fig. 3.8, the net effect of the trapped cells on the S parameters is on the order of 0.1 dB. The reference signal is also periodically taken for the purpose of monitoring the stability of the entire setup.

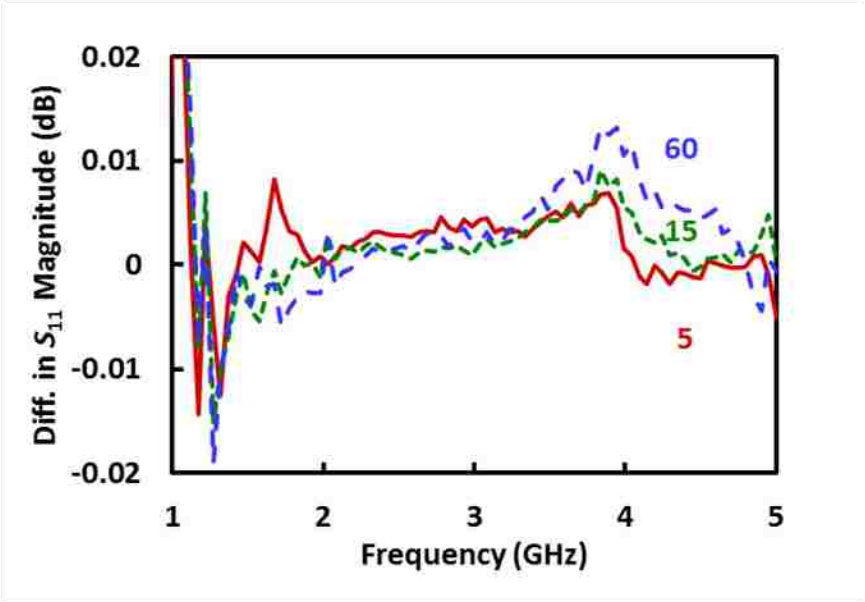

Fig. 3.8 Drift in the magnitude of S_{11} 5, 15 and 60 min after calibration without any cell trapped with improved measurement protocol.

3.4.2. Viability

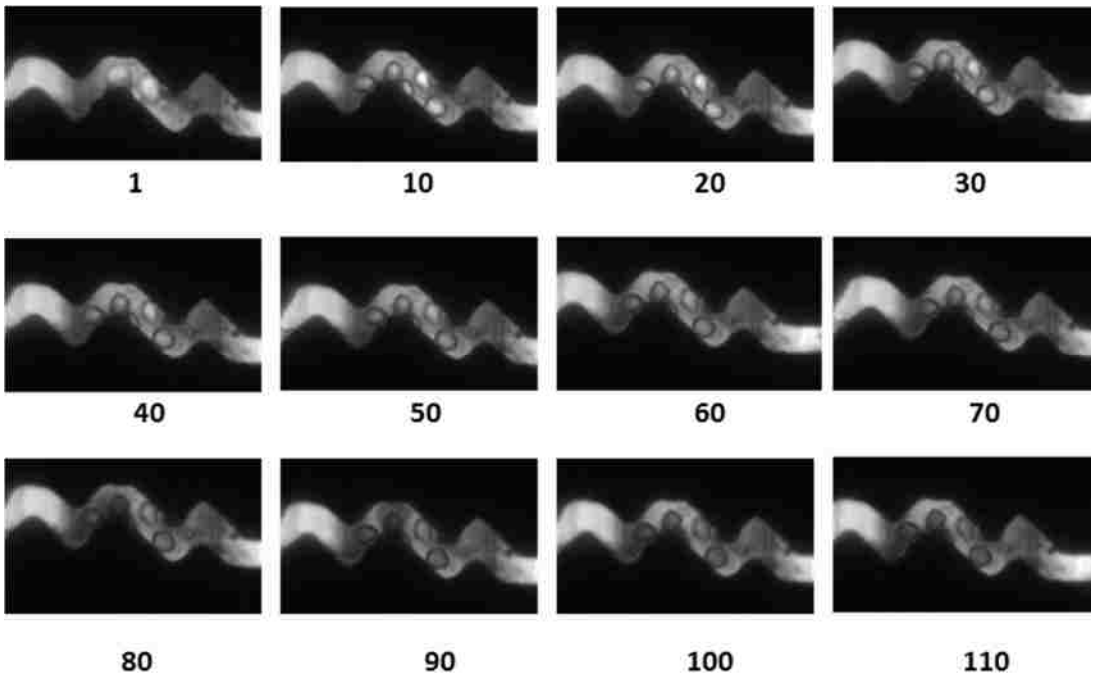

Fig. 3.9 Viability test with cell trapped in the channel and 1.5V DEP signal at 10MHz turning on over 120 min.

Although dielectrophoresis signals of comparable frequency and strength were used for trapping and found to have little effect on cell morphology or vitality [14][15], we observe sometimes that the cells die on chip and hard to remove and clean after they die. Thus on-chip viability test were done to study this influence. Fig. 3.9 shows pictures of an over-120-min viability test. After the cells get trapped in the target region, we keep the flow running and also a 1.5V DEP signal at 10MHz is on during the test. Also trypan blue dye is added to verify the cell live or dead condition on chip. It is apparent to observe that at the very beginning, the cells are round and bright which indicates they are alive. Later as time flies by, they are turning dark due to the fact that dead cells are taken the trypan blue dye and become darker in color. So that we confirm that the cells die faster in the channel compared with in the syringe or tube. The teeth region where has a higher E-field

and higher gradient of E-field seems accelerate cells dying speed. Long-time exposure in the microfluidic channel could be another reason.

Note about the viability issue, in our regular measurement, trapped cells will not be kept in the gap of CPW for too long time but within a measurement less than 3 min depending on the chosen IF bandwidth. Also, a low-speed flow is kept on during any measurement to both flush the leaking ions away and also provide enough air and liquid for cells to keep alive.

References

[1] H. E. Ayliffe, A. B. Frazier, and R. D. Rabbitt, "Electric impedance spectroscopy using microchannels with integrated metal electrodes," J. Microelectromechanical Syst., vol. 8, no. 1, pp. 50–57, Mar. 1999.

[2] S. Gawad, K. Cheung, U. Seger, A. Bertsch, and P. Renaud, "Dielectric spectroscopy in a micromachined flow cytometer: theoretical and practical considerations," Lab A Chip - LAB CHIP, vol. 4, no. 3, pp. 241–251, 2004.

[3] X. Cheng, Y. Liu, D. Irimia, U. Demirci, L. Yang, L. Zamir, W. R. Rodríguez, M. Toner, and R. Bashir, "Cell detection and counting through cell lysate impedance spectroscopy in microfluidic devices.," Lab Chip, vol. 7, no. 6, pp. 746–55, Jun. 2007.

[4] J. Chen, Y. Zheng, Q. Tan, Y. L. Zhang, J. Li, W. R. Geddie, M. A. S. Jewett, and Y. Sun, "A microfluidic device for simultaneous electrical and mechanical measurements on single cells," Biomicrofluidics, vol. 5, no. 1, p. 014113, Mar. 2011.

[5] K. Foster and H. Schwan, "Dielectric properties of tissues and biological materials: a critical review," Crit. Rev. Biomed. Eng., vol. 17, no. 1, pp. 25–104, 1989.

[6] C. Cheng-Hsin, W. Ching-Hua, H. You-Ming, C. Hsiang-Ching, and W. Chin-Hung, "Depth effects of DEP chip with mierocavities array on impedance measurement for live and dead cells," 3rd IEEE Int. Conf. Nano/Micro Eng. Mol. Syst. NEMS, pp. 858–863, 2008.

[7] Y. Feldman, R. Nigmatullin, E. Polygalov, and J. Texter, “Fractal-polarization correction in time domain dielectric spectroscopy,” Phys. Rev. E, vol. 58, no. 6, pp. 7561–7565, Dec. 1998.

[8] C. Merla, A. Denzi, A. Paffi, M. Casciola, G. d’Inzeo, F. Apollonio, and M. Liberti, “Novel passive element circuits for microdosimetry of nanosecond pulsed electric fields.,” IEEE Trans. Biomed. Eng., vol. 59, no. 8, pp. 2302–11, Aug. 2012.

[9] C. Palego, C. Merla, Y. Ning, C. R. Multari, X. Cheng, D. G. Molinero, G. Ding, X. Luo, and J. C. M. Hwang, “Broadband microchamber for electrical detection of live and dead biological cells,” in 2013 IEEE MTT-S International Microwave Symposium Digest, 2013, pp. 1–3.

[10] H.-L. Gou, X.-B. Zhang, N. Bao, J.-J. Xu, X.-H. Xia, and H.-Y. Chen, “Label-free electrical discrimination of cells at normal, apoptotic and necrotic status with a microfluidic device,” J. Chromatogr. A, vol. 1218, no. 33, pp. 5725–5729, Aug. 2011.

[11] H. Shafiee, M. B. Sano, E. A. Henslee, J. L. Caldwell, and R. V Davalos, “Selective isolation of live/dead cells using contactless dielectrophoresis (cDEP).,” Lab Chip, vol. 10, no. 4, pp. 438–45, Feb. 2010.

[12] R. Pethig and M. S. Talary, “Dielectrophoretic detection of membrane morphology changes in Jurkat T-cells undergoing etoposide-induced apoptosis.,” IET Nanobiotechnol., vol. 1, no. 1, pp. 2–9, Feb. 2007.

[13] A. Denzi, F. Apollonio, M. Liberti, M. Caterina, Y. Ning, C. Multari, C. Palego, X. Cheng, J. C. M. Hwang, and A. M. Description, “Cell Detection and Discrimination by a Microfluidic- Integrated Broadband Microchamber,” in European Microwave Conference, 2014, pp. 695–698.

[14] S. Archer, T. T. Li, a T. Evans, S. T. Britland, and H. Morgan, “Cell reactions to dielectrophoretic manipulation,” Biochem. Biophys. Res. Commun., vol. 257, no. 3, pp. 687–698, 1999.

[15] C. Huang, C. Liu, J. Loo, T. Stakenborg, and L. Lagae, “Single cell viability observation in cell dielectrophoretic trapping on a microchip,” Appl. Phys. Lett., vol. 104, no. 1, 2014.

Chapter 4. Broadband Electrical Detection of Biological Cells

4.1. Introduction

To resolve the dilemma of cell clogging or solution parasitics encountered by Coulter counters and to evolve a general-purpose electrical detection technique, broadband microwave measurements are used to overcome electrode polarization, AC dielectrophoresis to precisely place cells between narrowly spaced electrodes, and relatively wide microfluidic channels to prevent cell clogging. This unique combination of approaches results in reproducible sensing of single Jurkat and HEK cells, both live and dead, of different cultures at different times.

In this chapter, the detailed experimental demonstration and model of the broadband biological cells detection system are going to be discussed. The entire system setup is introduced in Section 4.2, followed by a description of measurement protocol in Section 4.3. In Section 4.4, the measurement results show linear relationship verse number of cells trapped, which prove the reproducible sensing of single cells. Section 4.5 discusses the equivalent circuit model for the detection system. Finally, Section 4.6 demonstrates the improved broader band design based on wafer measurement.

4.2. System setup

Fig. 4.1 shows the present test setup is comprised of electrical equipment and also microfluidic parts. An inverted fluorescent microscope (Nikon Eclipse TE2000-U) is used to allow simultaneous microwave measurement and visual validation. A vector network

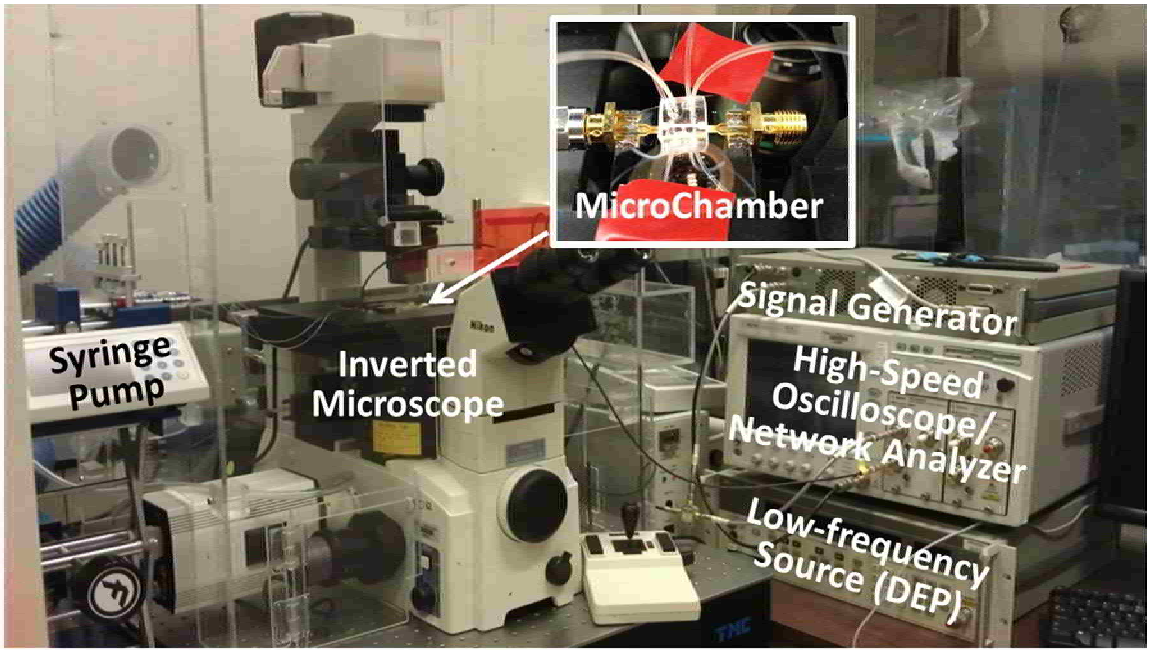

Fig. 4.1 Experiment setup.

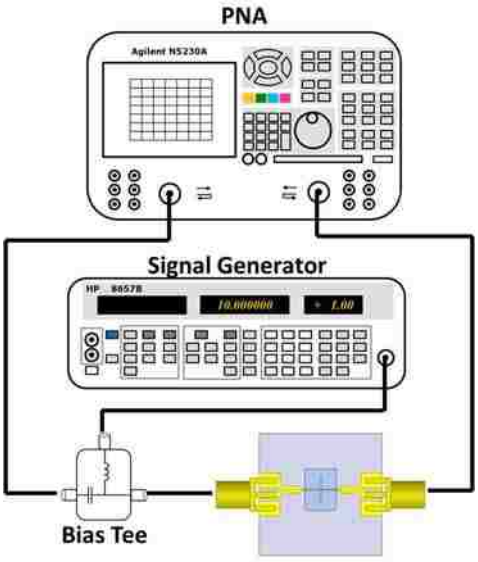

Fig. 4.2 System configuration of a frequency-domain measurement. Keysight (Agilent) N5230A Network Analyzer and Keysight (Hewlett-Packard) 8657B Signal Generator are included.

analyzer Keysight (Agilent) PNA N5230A is used for measuring the two-port scattering (S) parameters from 10MHz to 20GHz, which includes both the transmitted and reflected

signal. The applied setting of the PNA are IF bandwidth at 5Hz, no average and 201 data points in total. A low IF bandwidth is picked for its high accuracy during the entire sweep and it takes 2–3 minute for the current sweep.

For trapping the biological cells, a DEP signal of 10 MHz and 3 V was generated by a Keysight (Hewlett-Packard) 8657B Function Generator and coupled to the CPW via an Keysight (Agilent) 11612A Bias Network. Theoretically, the bias tee can be viewed as an idea capacitor and together with ideal inductor, however, there is a range of AC signal that can pass the inductor without being fully blocked. Checked with spectrum analyzer, the 10MHz signal can be more than 90% transmitted through the bias tee, however, it somehow limits the lower frequency of the S parameter measurement to 500 MHz.

The flow through the microfluidic channel is controlled by a syringe pump. A fixed rate of 0.05ul/min – 0.1ul/min is normally applied due to the consideration of small pressure in the microchannel and easy to trap the cells that flowed by the CPW region. Solution is injected from syringe pump through tubes to the sensor chip.

Fig. 4.3 shows the present microchamber for broadband detection is formed

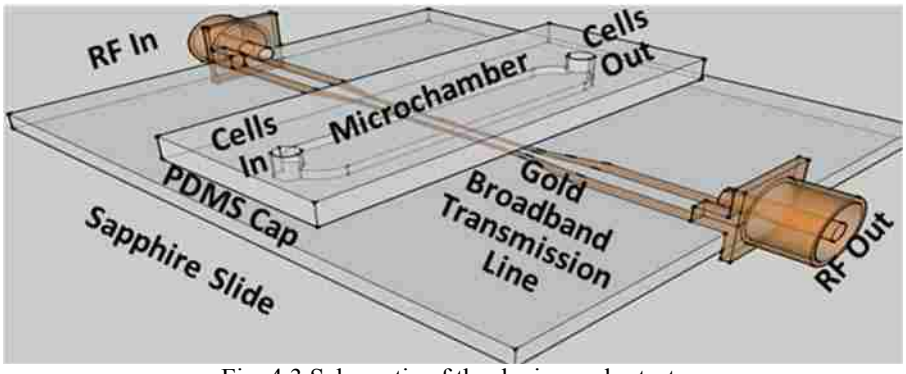

Fig. 4.3 Schematic of the device under test.

between a gold coplanar stripline fabricated on a sapphire slide and a microfluidic channel fabricated in a polydimethylsiloxane (PDMS) cover. The stripline is made of 2-μm-thick gold deposited on a 635-μm-thick sapphire microscope slide. The two electrodes of the stripline are approximately 100-μm wide and 10-μm apart inside the microchamber. The input and output of the stripline are terminated in SMA coaxial connectors affixed to opposite edges of the sapphire slide. This allows two-port scattering (S) parameters of a microwave signal of 1-5 GHz to be conveniently measured by using a vector network analyzer, after careful calibration with coaxial precision impedance standards. In general, microwave vector network analyzers have better sensitivity and dynamic range than impedance analyzers used at lower frequencies.

The microfluidic channel delivers single cells precisely. The microfluidic channel is approximately 50-μm high and 150-μm wide, which is patterned in a 2-mm-thick and 8-mm-wide PDMS cover then attached to the sapphire slide at a right angle to the stripline. The smaller overlap of the PDMS with the electrodes will reduce the loss along the CPW and deliver more signal to the target region.

4.3. Measurement Protocol

Electrically measurement usually involves two parts: trapping and sensing of the biological cells. Dielectrophoresis signals of comparable frequency and strength are used for trapping. It is found to have little effect on cell morphology or vitality [1], [2]. Typically, microwave measurements are performed with different numbers of cells repeatedly trapped and released by turning the dielectrophoresis signal on and off conveniently.

As shown in Fig. 4.4 , once the DEP signal is turned on, the cells start to be trapped in the gap region of the CPS electrodes which is the opaque region in the figures. After a

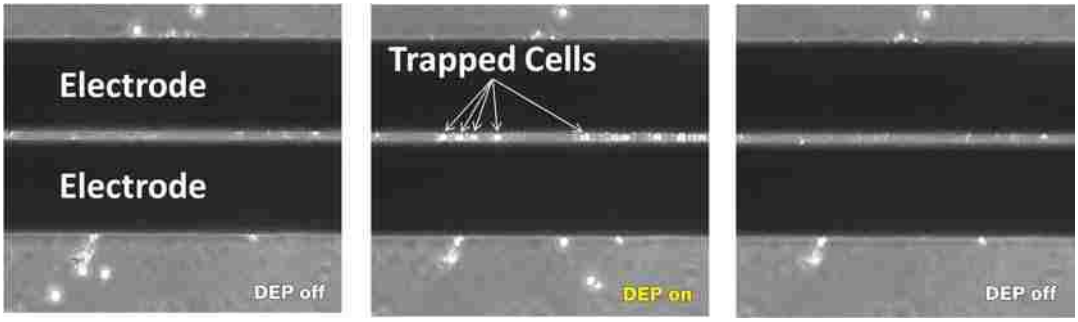

Fig. 4.4 The cell trapped with DEP force can be observed under microscope.

measurement is performed with 1 to 20 cells trapped, the dielectrophoresis signal is turned off to allow the trapped cells to be washed away. Then the measurement is repeated without any cell trapped so that the difference between the two consecutive measurements can be regarded as the net effect of the trapped cells even if the calibration drifts with time. This is critical because, although the calibration does not drift by more than 0.01 dB per hour, the net effect of the trapped cells on the S parameters is on the order of 0.1 dB.

Note that a vector network analyzer measures S parameters by comparing the reflected (S_{11}) or transmitted (S_{21}) signals with the incident signal and typically records their magnitudes in decibel (dB). Thus, S parameters are ratios to begin with, and the difference between two S parameters is also a ratio in decibel. By subtracting of the S-parameter of the chip with cells trapped between the electrodes from the one without cells, the difference which is the effect of the cells can be found. A linear region of difference regarding the variation number of cells has been highlighted, from 2GHz to 3.5GHz. The

slope of the linear regression, also represents the dispersion of S-parameter is further plotted for different number of cells for both live and dead Jurkat cells.

4.4. Measurement Results

Trapping is not only observable under the microscope, but also noticeable by the instant change in the S parameters monitored on the vector network analyzer. After data analysis according to Section 4.3, the results are shown as follows.

Fig. 4.5 (a) and Fig. 4.6(a) show that, with increasing number of live Jurkat cells trapped, the S_{11} magnitude mostly decrease while the S_{21} magnitude mostly increases. Meanwhile Fig. 4.5 (b) and Fig. 4.6 (b) show that the S_{11} and S_{21} phases mostly increase. Since the measurement overall behaviors of the S parameters is rather complicated as they are heavily influenced by resonances caused by the intrinsic circuits as well as the parasitic, and the increases or decreases of the S parameters may actually reverse signs across the band. Nevertheless, the decrease in S_{11} magnitude and increase in S_{21} magnitude are the most prominent and consistent between 2 GHz and 3.5 GHz. In either case, the dispersion between 2 GHz and 3.5 GHz appears to be linear so that, instead of focusing on any discrete frequency, linear regression was performed between 2 GHz and 3.5 GHz and the resulted dispersion magnitude used to quantify the net effect of the trapped cells on the S parameters. This is another advantage of broadband measurements over measurements at discrete frequencies.

With confirmation of the cell response relates to the different number of live Jurkat cells, we further studied the effect of the conditions of the cells like live or dead. Fig. 4.7 shows the results of the S parameter dispersion, which is the slope of the linear regress, as

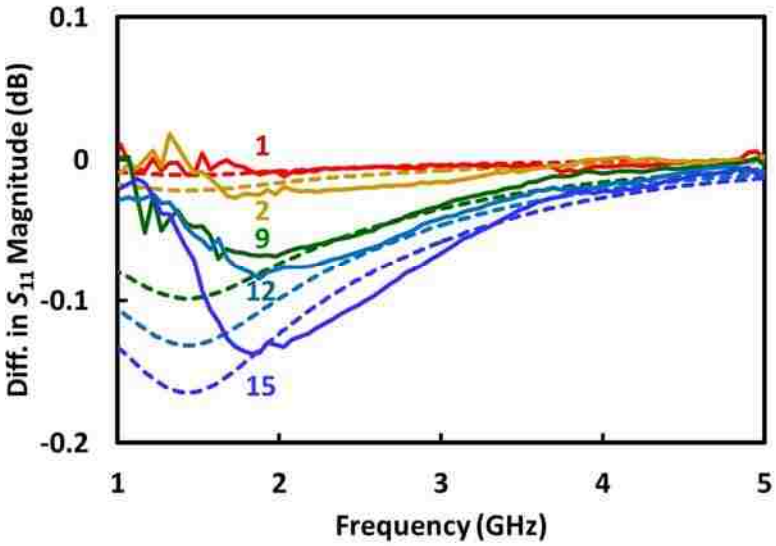

(a)

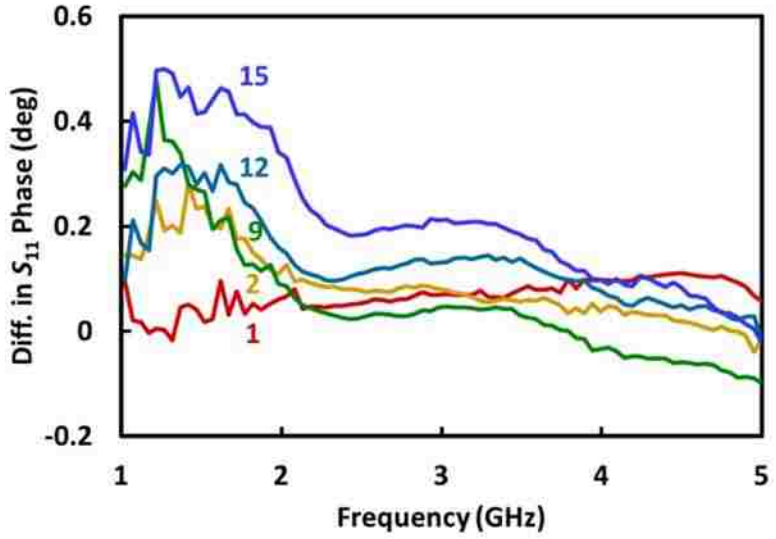

(b)

Fig. 4.5 Measured differences in the (a) magnitude of S_{11}, (b) phase of S_{11} with 1, 2, 9, 12, and 15 live Jurkat cells trapped. Dashed curves are simulated by the model shown in Equivalent circuit model used to deembed cytoplasm resistance R_C and capacitance C_C from the solution effect and the parasitic impedance.Fig. 4.9Fig.

in both live and dead Jurkat cells. Limited by the gap region of the electrodes, as well as the difficulty in visually counting the cells once a huge group of cells get together layer by layer, the number of cells trapped is being controlled no more than 20. The focus plane of the microscope has to been adjusted every time during cell counting to get precise cell

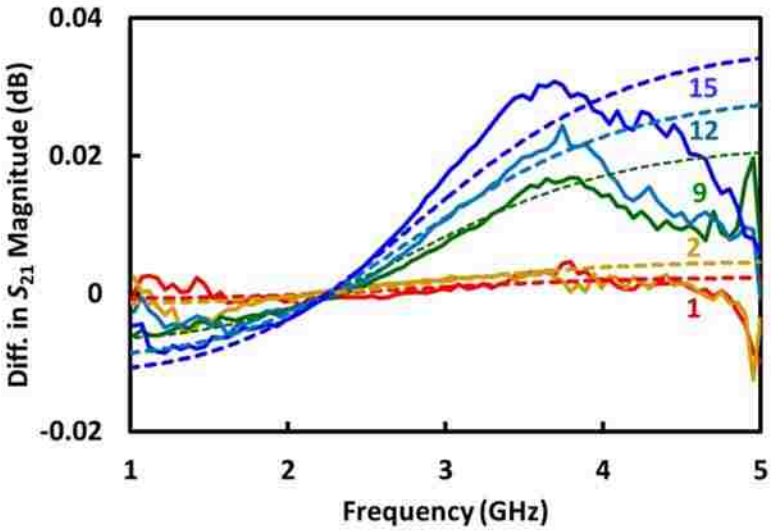

(a)

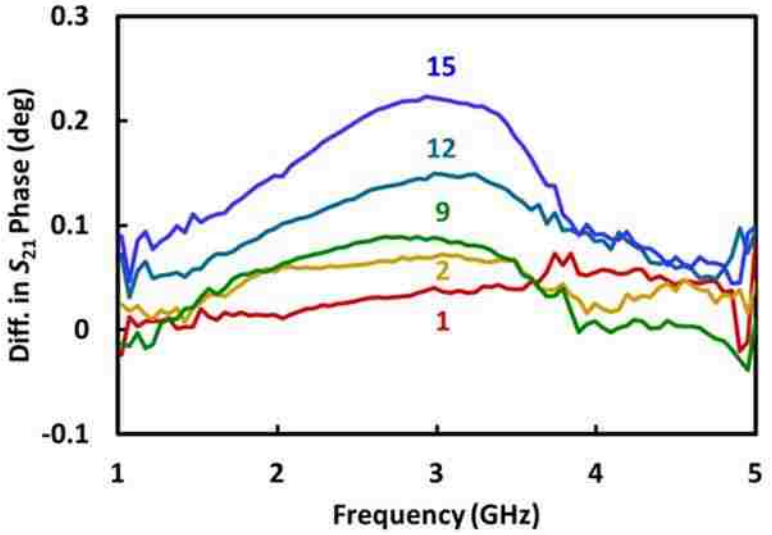

(b)

Fig. 4.6 Measured differences in the (a) magnitude of S_{21}, (b) phase of S_{21} with 1, 2, 9, 12, and 15 live Jurkat cells trapped. Dashed curves are simulated by the model shown in Fig. 4.9.

numbers. The error bar due to the system drift is also plotted in the figure.

As pointed out from the figures, measurements are conducted during different days, and some of them in different months. Every measurement in a day means an entirely new bonding of PDMS together with the chip after cleaning with alcohol and DI water, a

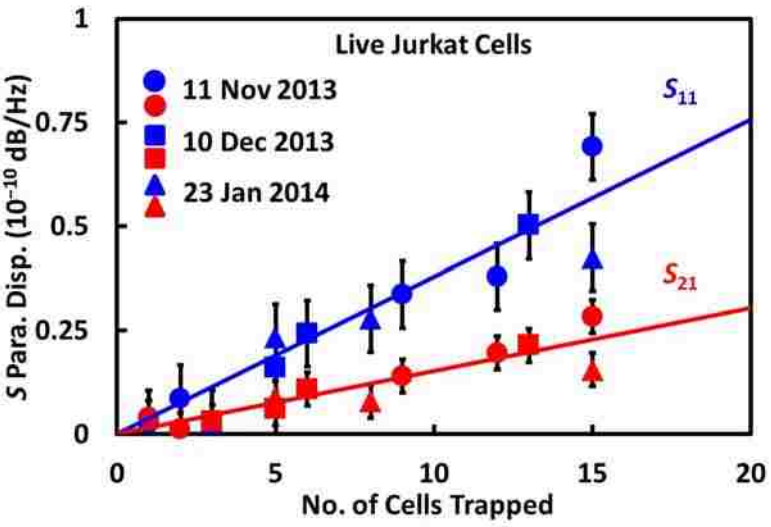

(a)

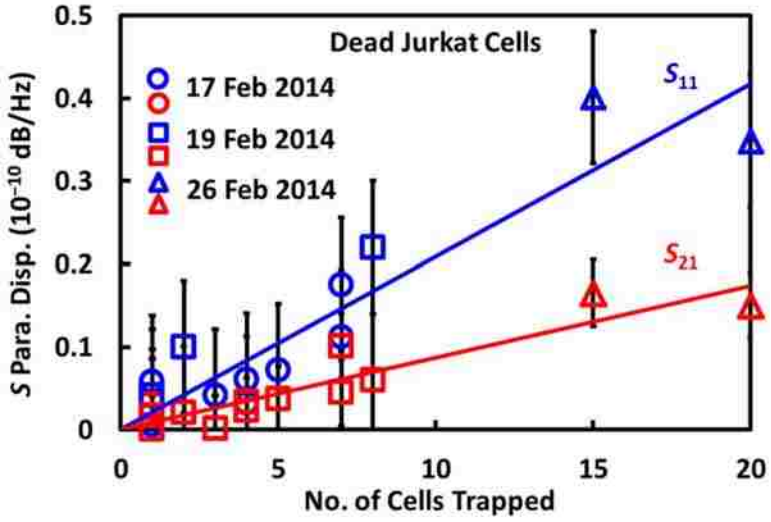

(b)

Fig. 4.7 Measured changes in S-parameters dispersion between 2 GHz and 3.5 GHz for repeated experiments with different numbers of (a) live and (b) dead Jurkat cells trapped.

new electrical connection and calibration. Thus it indicates the high repeatability of the experiments and the self-consistency. The S parameter dispersion is in good linear relationship versus number of cells that trapped at the target gap region.

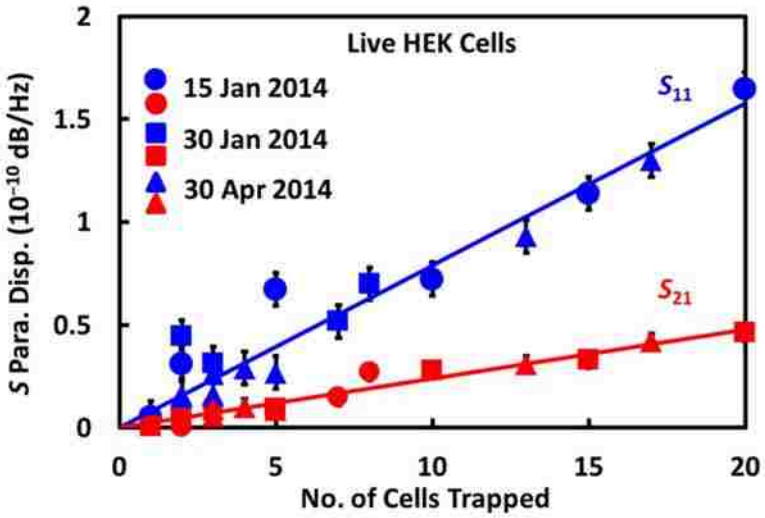

(a)

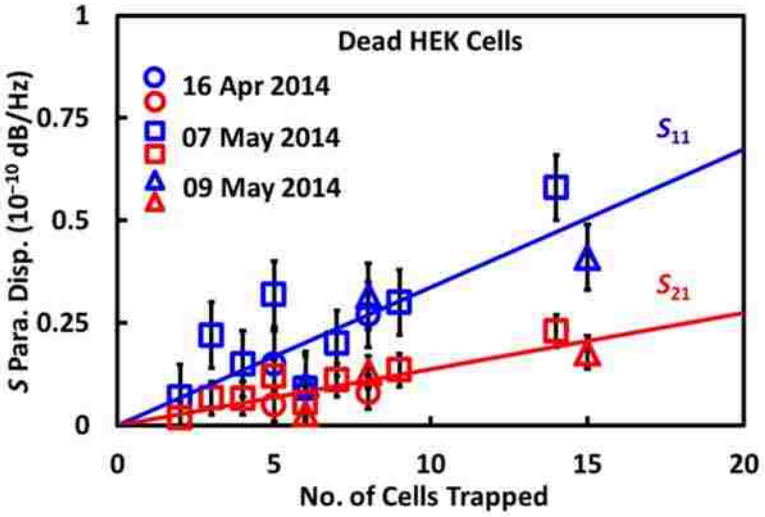

(b)

Fig. 4.8 Measured changes in S-parameters dispersion between 2 GHz and 3.5 GHz for repeated experiments with different numbers of (a) live and (b) dead HEK cells trapped.

We then tried on another type of mammalian cells, which is the HEK cell to fully study the cell performance with the same setup. Fig. 4.8 shows the measured changes in S-parameters dispersion for live and dead HEK cells. From the figure, we can see that the HEK cells have a similar response with the Jurkat cells.

In all, Fig. 4.7 and Fig. 4.8 show the measured changes in S-parameter dispersion are not only proportional to the number of cells trapped down to the single-cell level, but also reproducible for cells cultured and trapped in different months. Although the dispersion in S_{11} is greater than that in S_{21}, the magnitude of S_{11} is also greater than that of S_{21}. Therefore, the net effect of the trapped cells on S_{11} is comparable to that on S_{21}. Qualitatively, S-parameter dispersions of Jurkat and HEK cells have similar trends. Quantitatively, S-parameter dispersions of HEK cells is approximately twice that of the Jurkat cells, which is consistent with HEK cells being approximately twice the size of Jurkat cells. For both types of cells, the effects of dead cells are much weaker than that of the live cells. For a single dead cell, the effect approaches the noise floor. The reason for the different effects shown here is analyzed and discussed in next section.

4.5. Circuit Model and Discussion

In the simplest model, the electrical properties of a cell can be represented by a series R-C equivalent circuit comprising the cytoplasm resistance and the membrane capacitance. However, at microwave frequencies, the impedance associated with the cytoplasm resistance is much larger than that associated with the membrane capacitance. As mentioned earlier, the former is on the order of 10^5 Ω, whereas the latter is on the order of 50 Ω. Thus, the membrane capacitance is mostly bypassed and the remaining capacitance associated with the cytoplasm is best represented by a parallel R-C equivalent circuit of the cytoplasm resistance R_C and cytoplasm capacitance C_C. However, this simple model is complicated by the solution effect and the parasitic impedances.

To de-embed the cytoplasm resistance and capacitance from the solution effect and the parasitic impedances, a 1-D mixture model is used instead of the commonly used Maxwell 3-D mixture theory, because the latter applies only to low cell-to-sample volume ratios. Fig. 4.9 shows that the model comprises equivalent circuits for the trapped cells, the undisplaced solution, the microchamber, the transition, and the coplanar stripline, respectively. The trap between the electrodes is divided into 20 cubes of 10^3 μm^3 each.

Initially, without any cell trapped, the trap is represented by 20 R_S-C_S subcircuits in parallel, where R_S and C_S are the resistance and capacitance of 10^3 μm^3 of solution. After N cells are trapped, the trap is represented by N R_C-C_C subcircuits in parallel with (20 – N) R_S-C_S subcircuits. The total parallel resistance R_P and capacitance C_P are

$$R_P = \frac{R_C R_S}{(20-N)R_C + NR_S}, \quad C_P = NC_C + (20-N)C_S \qquad (4.1)$$

R_P and C_P can then be used by a circuit simulator to fit the measured S-parameters dispersion. Fig. 4.9 shows also that the microchamber is represented by transmission lines

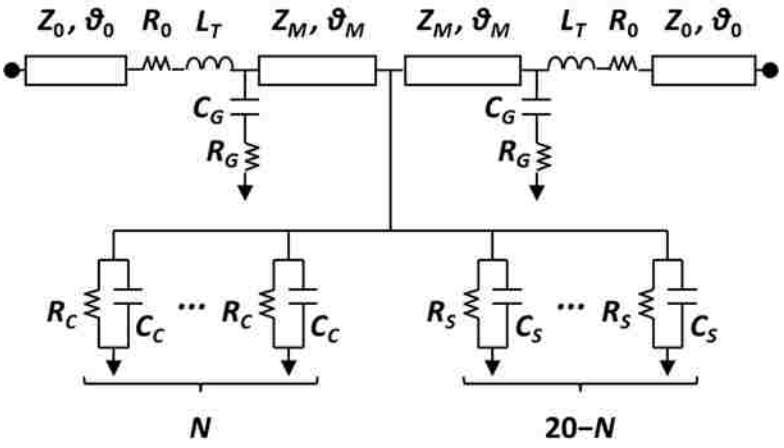

Fig. 4.9 Equivalent circuit model used to deembed cytoplasm resistance R_C and capacitance C_C from the solution effect and the parasitic impedance.

of characteristic impedance Z_M and electrical length θ_M with grounding parasitics through R_G and C_G and transitions of L_T. Outside the microchamber, the coplanar stripline is represented by transmission lines of characteristic impedance Z_0, electrical length θ_0, and loss R_0. The analysis confirmed that, at these microwave frequencies, the electrode polarization effect is negligible hence not represented in the equivalent circuit.

Table 4.1 lists the extracted equivalent-circuit parameter values for live and dead Jurkat cells. The equivalent circuit of Fig. 4.9 was implemented in the ADS circuit simulator, as shown in Fig. 4.10, initially with estimated parameter values, then the S parameters simulated by using the equivalent circuit were compared with the measured ones and the parameter values iteratively adjusted for the optimum fit between simulated and measured S parameters. Fig. 4.11 illustrates the optimized fit without any cell trapped. The fit with different numbers of live Jurkat cells trapped are illustrated in Fig. 4.5(a) and Fig. 4.5(c) where the simulated S-parameter magnitudes are plotted in dashed curves.

Table 4.1 Equivalent-Circuit Parameter Values

Subcircuit	Parameter	Symbol	Jurkat		HEK	
			Live	Dead	Live	Dead
Cell	Cyto.Resistance	R_C (kΩ)	190	860	120	500
	Cyto.Capacitance	C_C (fF)	29			
Solution	Unit Resistance	R_S (kΩ)	480			
	Unit Capacitance	C_S (fF)	30			
Micro-chamber	Char. Impedance	Z_M (Ω)	28			
	Length @ 3 GHz	θ_M (°)	5			
Ground	Resistance	R_G (Ω)	4.1			
	Capacitance	C_G (fF)	420			
Transition	Inductance	L_T (nH)	1.7			
Stripline	Char. Impedance	Z_0 (Ω)	55			
	Length @ 3 GHz	θ_0 (°)	12			
	Loss	R_0 (Ω)	6.5			

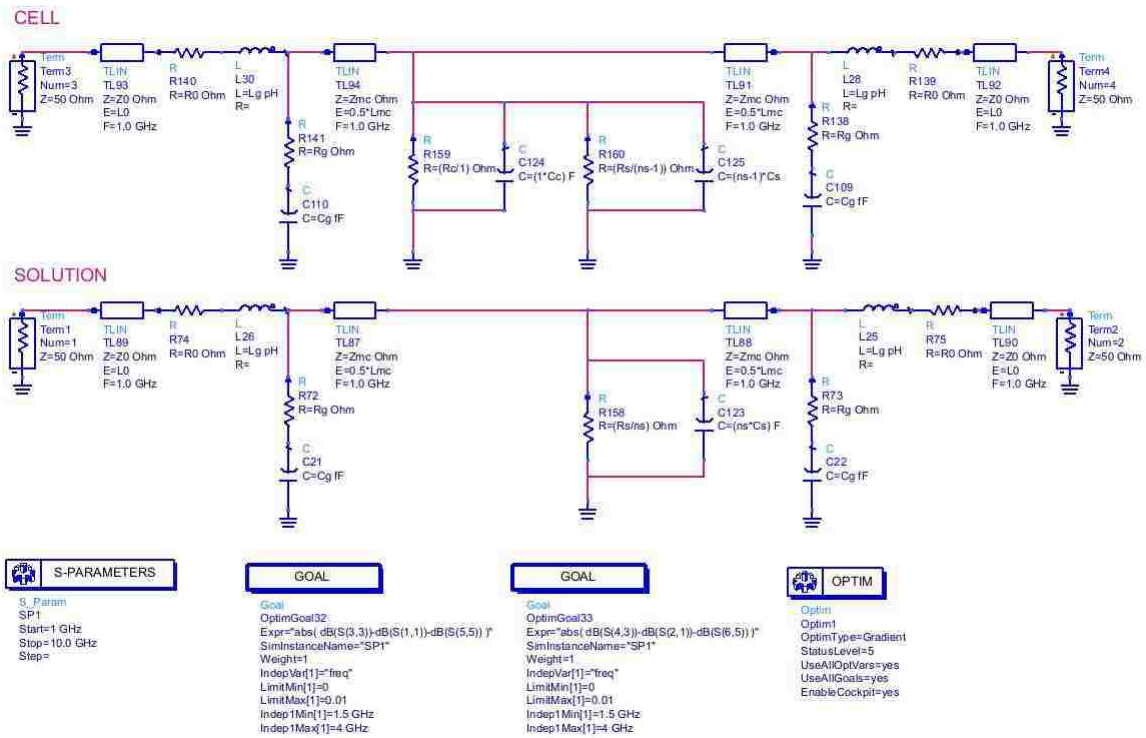

Fig. 4.10 Model implementation in Keysight Advance Design System (ADS).

Although not shown in in Fig. 4.5(b) or Fig. 4.5(d), the fit of the S-parameter phases exhibit comparable fit, albeit over a narrower bandwidth.

The equivalent-circuit parameter values can be estimated as in the following. The resistivities of cytoplasm and sucrose are on the order of 1 Ω·m [3] and 10 Ω·m [4], respectively, which imply the resistances of 10^3 μm^3 of cytoplasm and sucrose should be on the order of 10^5 Ω and 10^6 Ω, respectively. This is consistent with the optimized R_C and R_S values listed in Table I except that their difference is less than an order of magnitude, probably because the round cells do not completely displace the solution in a 10^3 μm^3 cube. (In any case, the 10^3 μm^3 volume is overestimated because, although the electrodes are spaced 10 μm apart, they are only 2 μm thick. Considering the fringing field, the actual unit volume should be closer to 10 μm × 10 μm × 3 μm than 10^3 μm^3.) This can also

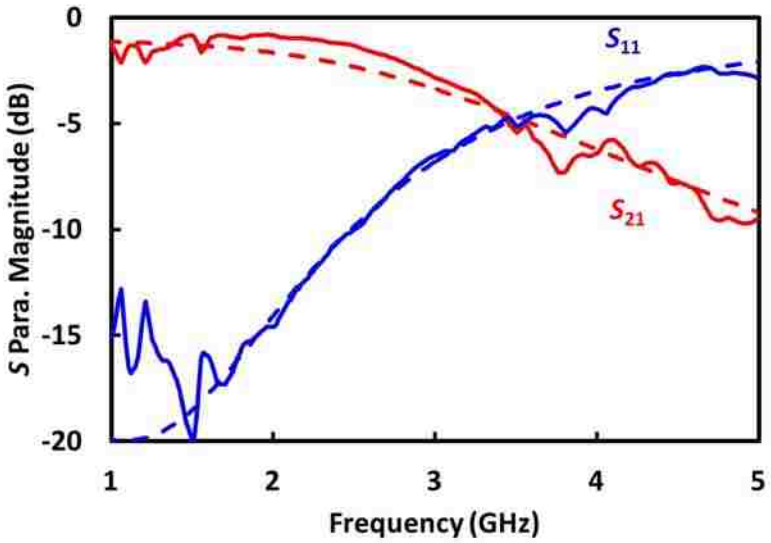

(a)

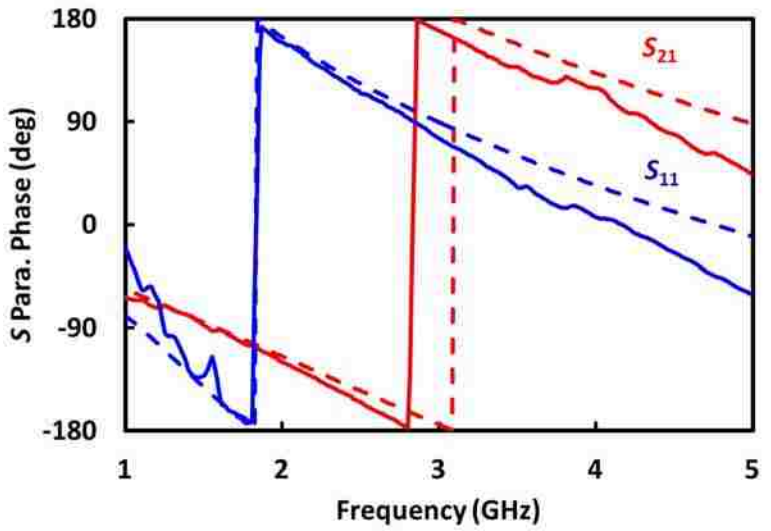

(b)

Fig. 4.11 Measured (solid curve) versus simulated (dashed curve): (a) magnitudes and (b) phase of S_{11} and S_{22} without any cell trapped.

explain the smaller R_C extracted for the live HEK cells than that of the live Jurkat cells, because the larger HEK cells can more completely displace the solution between the electrodes. As the cells die, they lose their ionic content and, hence, the cytoplasm conductivity. This can explain the much higher R_C extracted for the dead Jurkat and HEK cells, which is shown in Fig. 4.12. Both the cytoplasm and the sucrose solution are

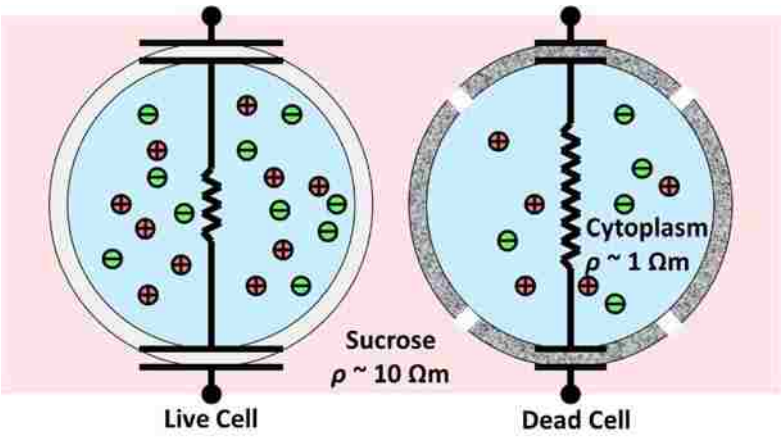

Fig. 4.12 Explanation of the difference of the capacitance and resistance in live and dead biological cells

mostly made of water. The capacitance of 10^3 μm^3 of water sandwiched between two 10^2 μm^2 electrodes is approximately 10 fF, which is on the same order as the extracted C_C and C_S. Other than R_C, R_S, C_C and C_S, the remaining equivalent-circuit parameters were estimated from the physical dimensions and properties of PDMS, gold and sapphire.

The observed decrease in S_{11} magnitude and increase in S_{21} magnitude can be understood intuitively, although the overall behaviors across the band is rather complicated and can only be simulated by the equivalent circuit. Between 2 GHz and 3.5 GHz, the overall microchamber impedance is less than 50 Ω. When the solution is replaced by the trapped cells with lower resistance and capacitance, the microchamber impedance becomes closer to 50 Ω, which results in less reflection (smaller S_{11} magnitude) and better transmission (larger S_{21} magnitude) of the microwave signal. Meanwhile, the lower capacitance causes less delay of the microwave signal, hence, relatively higher S_{11} and S_{21} phases as shown in Fig. 4.5.

The above work, as in [5], confirms that a cell response in the frequency domain can be measured with different number of cells and different condition (live/dead) of cells

in both Jurkat and HEK cells. However with the current the measurement setup, the sensitivity is limited. Thus, an improved setup and protocol is put forward for further study.

4.6. Improved Broader Band Design

Although accuracy, reproducibility and linear dependence on the number of cells were demonstrated in the previous sections, reliable bandwidth is limited to 2−3.5 GHz. The improved detection technique introduced in [6] extends the reliable bandwidth for electrical detection of individual cells up to 20 GHz by using a homemade probe station in conjunction with a carefully optimized coplanar waveguide (CPW), closely spaced microwave probes, and frequent calibrations to move the reference planes next to the microfluidic channel.

Fig. 4.13(a) demonstrates the setup with the homemade microwave probe station on top of the inverted microscope. This system combines both the probe station for precise electrical measurement together with the inverted microscope from which the cell movement in the microfluidic channel can be visually observed. The probe positioners are put onto a thick aluminum board which has a cutting area in the middle for the microscope region. The front of the probe positioners are added with a man-made aluminum extension to adjust the height and the distance of the probes, as shown in Fig. 4.13(b). The piece on top of the chip area is the microscope's illumination pillars including condensers. A stereoscope is used to assist the probing.

Fig. 4.14 (a) shows schematically that the test chip is based on a gold CPW sandwiched between a quartz substrate and a polydimethylsiloxane (PDMS) cover. The 2-μm-thick gold CPW has a 40-μm-wide center electrode that is flanked by two 100-μm-

(a)

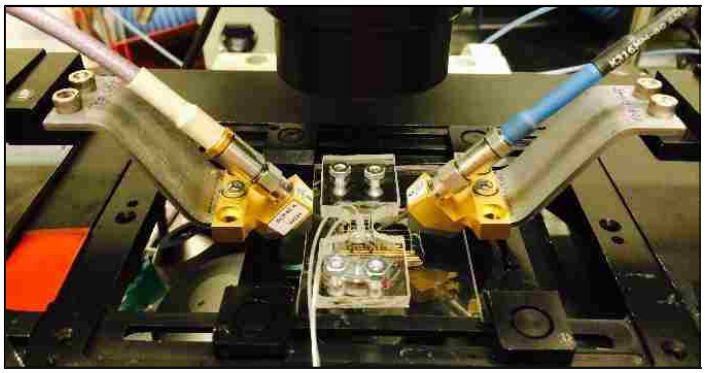

(b)

Fig. 4.13 Homemade microwave probe station on top of inverted microscope (a) side view (b) front view

wide ground electrodes. The gap between the center electrode and either ground electrode is 10-μm wide. The quartz substrate is 635-μm thick. The PDMS cover is 5-mm wide and 5-mm high with a microfluidic channel of 150-μm wide and 50-μm high etched into its underside. The microfluidic channel intersects the CPW perpendicularly with three inlets on one end and one outlet on the other end. Buffer solution flowing through the side inlets at the inlet end is used to steer the flow of cell suspension through the center inlet. Fig. 4.14 (b) shows the micrograph of the portion of the CPW under the microfluidic channel with cells trapped by DEP between the center and ground electrodes. The portion of the ground electrodes under the microfluidic channel is perforated to facilitate visual tracking of the

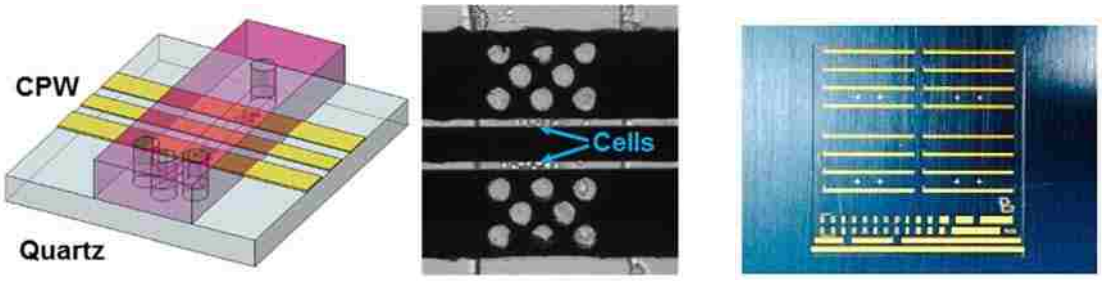

(a) (b) (c)

Fig. 4.14 (a) Schematic test chip based on a CPW sandwiched between quartz substrate and PDMS cover. (b) Micrograph of CPW showing trapped cells between center and ground electrodes. Holes in ground electrodes inside microfluidic channel facilitate tracking of cell flow. (c) Top view of the entire chip.

cells flowing above the electrodes, which would otherwise block the view through the inverted microscope. With a diameter of 30 μm, the perforations are much smaller than the microwave wavelength and hence, negligible as far as the electrical characteristics of the CPW is concerned. Fig. 4.14 (c) shows a top view of the entire design. Crossed marks has been put on the layout for alignment of gold electrode and PDMS cap.

The dimensions of the CPW, the PDMS cover, and the microfluidic channel are optimized by using the ANSYS HFSS 3D full-wave electromagnetic simulator as discussed in Section 2.2. Fig. 4.15 shows reasonable agreement between simulated and measured S parameters from 500 MHz to 20 GHz. With the microfluidic channel filled with aqueous solution, no in-band resonance is simulated or measured.

To extract the S parameters shown in Fig. 4.15 from the microwave measurement, 2-port short-open-load-through calibration with a Cascade Microtech 85052D calibration substrate was used to move the reference planes form the Keysight (Agilent) Technologies 5230A Precision Network Analyzer to the tips of the Cascade Microtech ACP40 GSG Probes. The resulted return loss $|S_{21}|$ is larger than 13 dB and the insertion loss $|S_{11}|$ is

smaller than 3 dB up to 20 GHz, even with a solution-filled channel.

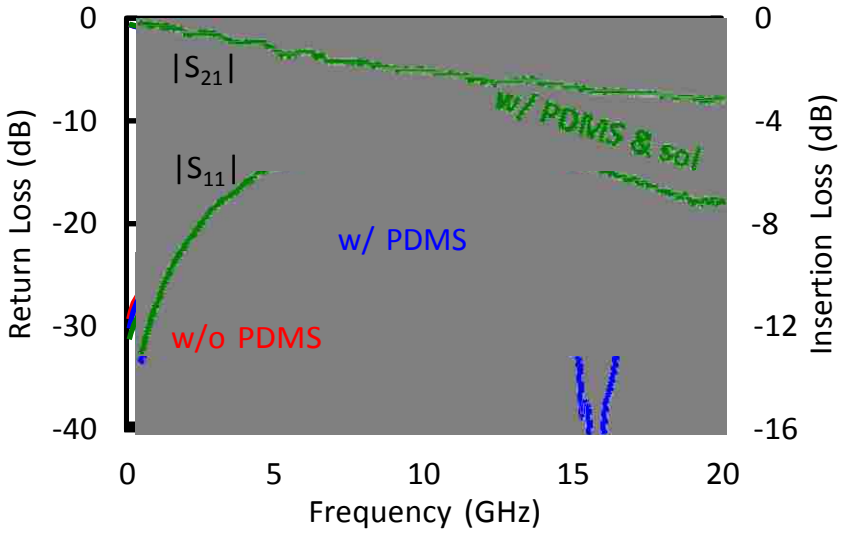

Fig. 4.15 Measured (solid curves) vs. simulated (dashed curves) return loss $|S_{11}|$ and insertion loss $|S_{21}|$ for the CPW (a) without PDMS cover, (b) with PDMS cover but empty microfluidic channel, and (c) with PDMS cover and microfluidic channel filled with aqueous solution.

Fig. 4.16 shows the measured differences in return loss $|S_{11}|$ and insertion loss $|S_{21}|$ as functions of the number of cells trapped. It can be seen that, as the solution in the detection volume is gradually displaced by the trapped cells, the CPW characteristic impedance increases towards 50 Ω resulting in better impedance match and hence lower $|S_{11}|$ and higher $|S_{21}|$. Further, the differences increase linearly with both the measurement frequency as well as the number of cells trapped as in previous sections. However, the linear trend occurs across the entire bandwidth of 0.5−20 GHz as opposed to being limited to 2−3.5 GHz. This allows the dispersion of the measured S parameters to be more reliably extracted for each number of cells trapped as shown in Fig. 4.17, although their magnitude are on the same order of magnitude of 10^{-11} dB/Hz as in [7]. Fig. 4.17 demonstrates also the reproducibility between measurements performed on different dates with different cell

cultures.

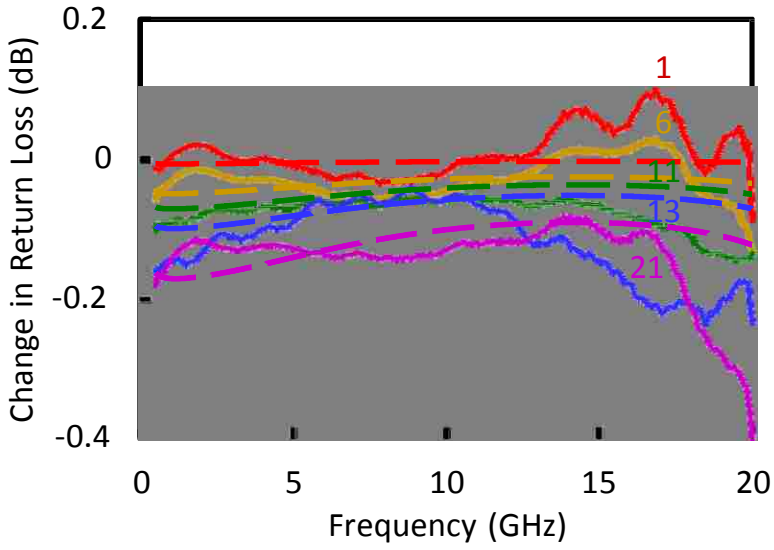

(a)

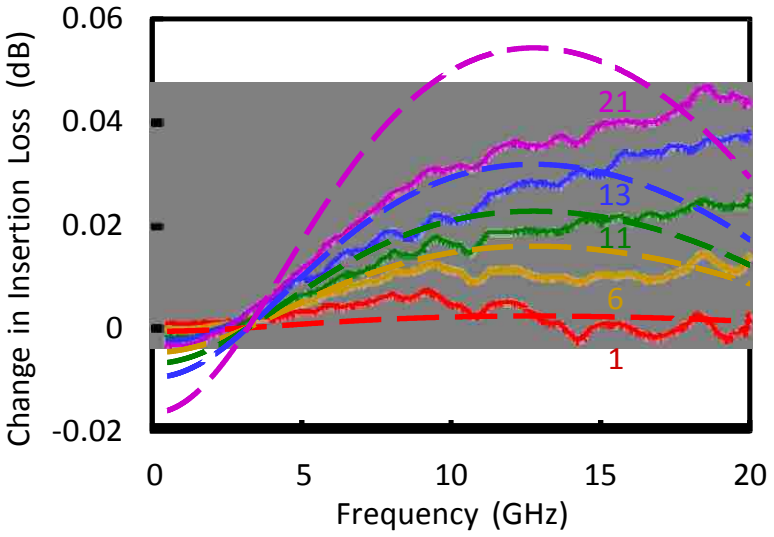

(b)

Fig. 4.16 Measured (solid curves) vs. modeled (dash curves) differences in (a) return loss |S11| and (b) insertion loss |S21| as functions of number of live Jurkat cells trapped.

For detailed quantitative analysis of the measured S parameters, an equivalent-circuit model similar to that of [7] was used. However, to account for the CPW dispersion across the present bandwidth of 0.5−20 GHz, it was necessary to make the CPW loss resistance R_0 frequency-dependent with a linear coefficient of 0.75×10^{-9} Ω/Hz. Using such

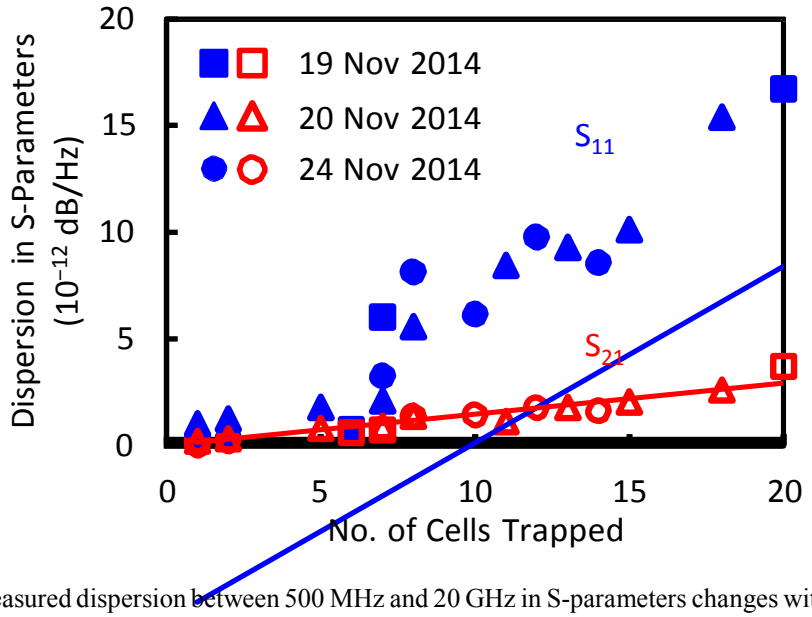

Fig. 4.17 Measured dispersion between 500 MHz and 20 GHz in S-parameters changes with different number of live Jurkat cells trapped.

a dispersive model, the extracted cytoplasm resistance of 190 kΩ is the same as that of [7] but valid over a much wider bandwidth.

Using probed instead of connectorized measurement, the bandwidth of cell detection was successfully extended from 2−3.5 GHz to 0.5−20 GHz with comparable sensitivity and reproducibility. With carefully optimized CPW, PDMS and channel, smooth and well-behaved S parameters were measured across the band. From the measured S parameters, the extracted cytoplasm resistance of 190 kΩ for a live Jurkat is consistent with the previously reported value but valid over a much wider bandwidth. This shows that the present technique can be used to reliably determine the broadband electrical characteristics of biological cells.

References

[1] S. Archer, T. T. Li, a T. Evans, S. T. Britland, and H. Morgan, "Cell reactions to dielectrophoretic manipulation," Biochem. Biophys. Res. Commun., vol. 257, no. 3, pp. 687–698, 1999.

[2] C. Huang, C. Liu, J. Loo, T. Stakenborg, and L. Lagae, "Single cell viability observation in cell dielectrophoretic trapping on a microchip," Appl. Phys. Lett., vol. 104, no. 1, 2014.

[3] I. Ermolina, Y. Polevaya, and Y. Feldman, "Analysis of dielectric spectra of eukaryotic cells by computer modeling.," Eur. Biophys. J., vol. 29, no. 2, pp. 141–145, 2000.

[4] K. Herold and A. Rasooly, Lab-on-a-Chip Technology: Biomolecular Separation and Analysis | Book. Caister Academic Press, 2009.

[5] Y. Ning, C. Multari, X. Luo, C. Palego, X. Cheng, J. C. M. Hwang, A. Denzi, C. Merla, F. Apollonio, and M. Liberti, "Broadband Electrical Detection of Individual Biological Cells," IEEE Trans. Microw. Theory Tech., vol. 62, no. 9, pp. 1905–1911, Sep. 2014.

[6] Y. Ning, C. Multari, X. Luo, X. Cheng, J. C. M. Hwang, A. Denzi, C. Merla, F. Apollonio, and M. Liberti, "Improved Broadband Electrical Detection of Individual Biological Cells," IEEE MTT-S Int. Microw. Symp. Dig., pp. 1–3, Jun. 2015.

[7] Y. Ning, C. Multari, X. Luo, C. Palego, X. Cheng, J. C. M. Hwang, A. Denzi, C. Merla, F. Apollonio, and M. Liberti, "Broadband Electrical Detection of Individual Biological Cells," IEEE Trans. Microw. Theory Tech., vol. 62, no. 9, pp. 1905–1911, Sep. 2014.

Chapter 5. Conclusion and Future Work

5.1. Conclusion of This Dissertation

This dissertation focuses on the study of the broadband detection of individual biological cells. After considering the electrical design, microfluidic integration and real-world problems, we have demonstrated the detection possibilities from time domain of nanosecond pulse, to frequency domain in KHz – MHz range, and finally GHz range. Special efforts are made to resolve the dilemma encountered by Coulter counters and evolve a general purpose electrical detection technique. We use broadband microwave measurement to overcome electrode polarization, AC dielectrophoresis to precisely place cells between narrowly spaced electrodes for maximum cell-to-sample volume ratio, and relatively wide microfluidic channels to prevent cell clogging. The detection technique presents detailed data and analysis at higher frequencies (GHz vs. MHz) to prove that the unique combination of these approaches can be reproducibly sensitive to single cells of different types, with different setups and in different days. The electric circuit model that generated from different electrode designs of CPW and CPS consistently extract the same value for the resistance of the cytoplasm. Further, simple analysis of the data confirms that microwave signals can penetrate through the cell membrane to probe the properties of cytoplasm.

5.2. Recommendation for Future Research

One of the future researches can be done on innovative calibration techniques specifically for microchamber system. In order to reach more general-purpose uses such as intracellular probing and separating different pathogens, broadband electrical detection

requires even better sensitivity and reproducibility. The improved calibration will push the sensitivity to sub-fF level and suitable for single cells detection.

Unlike the section by section characterization in [1], researchers have already started to explore along this way. In Fig. 5.1 (a), researcher [2] uses a compatible method with TRL calibration procedure and use the wave transmission matrices Thru and Tline to retrieve the dielectric property of the fluid in the microfluid section. In Fig. 5.1 (b), a two-tier calibration method is reported [3]. After a first-tier Thru-Reflect-Reflect-Match (LRRM) up to the probe tips, calibration with air, water and methanol constitutes the second-tier calibration, moving the reference plane from the probe-tips to LUT, with the two-port error boxes. Both work demonstrate the idea of moving the reference plane for a simplified measurement of the material-under-test. What's more, as in [4], by using a property model, the sensor boundary don't have to be precise but the parasitics or the

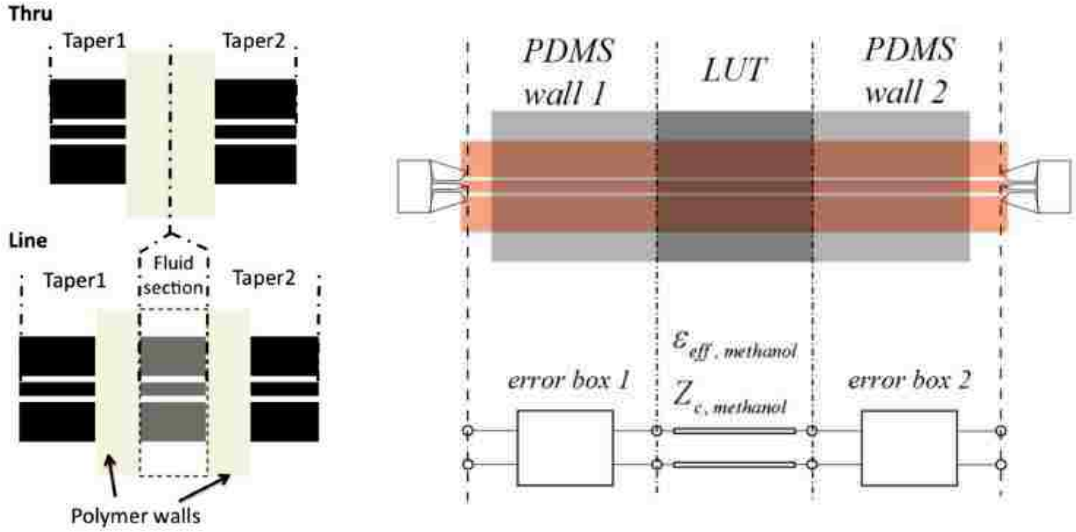

(a) (b)

Fig. 5.1 (a) Schematic views of the "thru" and "line" calibration element and the biosensor. (b) Error boxes and line parameters to be solved by calibration using reference materials. (– –) indicates the reference plane of the first-tier (LRRM) calibration and (–·–) indicates the reference plane of the second-tier calibration using reference liquids.

alignment inherent influence could be absorbed into considerations. The concept could be also useful for the biological cells measurement and detection. Thus, in addition to on-wafer TRL calibration standards, novel calibration techniques involving electronically controlled impedance standards and liquids of controlled dielectric properties could be explored.

Another interesting topic could be integration CMOS technology together microfluidics in biological cells detection. A lot of CMOS-based Lab-on-a-Chip research have already been done for years, as shown in Fig. 5.2. For example, techniques and methods of making either shallow or deep microchannels have been develop using the standard CMOS process [5]. Post-fabricated microfluidic channels on top of the IC chips to introduce biological cells to the chip surface and biological cells are manipulated by microscopic magnetic field [6]. A hybrid microsystem consist of heater and temperature sensor on CMOS together with multilayer PDMS for stand-alone cell culture and incubation [7]. A CMOS-based capacitive interface circuit was reported using TSMC 0.18 CMOS process and incorporating microfluidic channels [8]. Integrated circuit chip has been designed to trap and move individual living biological cells using DEP force[9]. Mentioned in [10], The choice of monolithic or hybrid integration of microfluidic and ICs, as shown in Fig. 5.3, is based on various applications.

The miniaturization and integration pulse the improvement of the signal-to-noise ratio [11] will bring CMOS-based Lab-on-a-Chip bio detection and differentiation a future market.

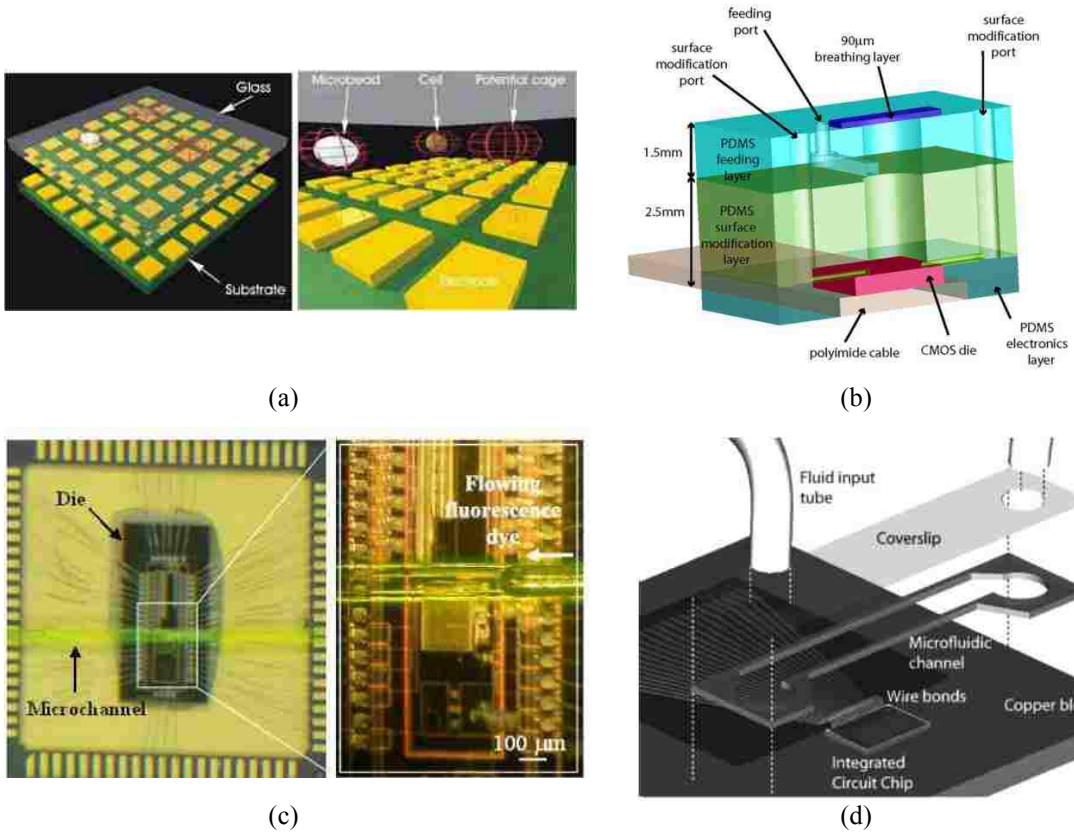

Fig. 5.2 (a) Sketch of the biochip section [6]. (b) Chip-scale incubator rendered in cross-sectional perspective [7]. (c) Optical microscopic image of microchannel fabricated by direct-write assembly technique and integrated on chip [8].(d) IC/microfluidic chip packaging scheme [9]. (e) Schematics of ICs and microfluidic networks integrations with monolithic configuration or a hybrid one including flip-chip or wire bonding of the ICs [10].

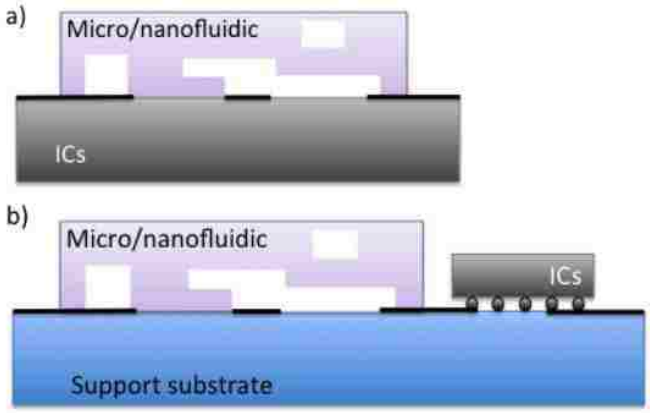

Fig. 5.3 Schematics of ICs and microfluidic networks integrations with monolithic configuration or a hybrid one including flip-chip or wire bonding of the ICs [10].

References

[1] J. C. Booth, N. D. Orloff, J. Mateu, M. Janezic, M. Rinehart, and J. A. Beall, "Quantitative Permittivity Measurements of Nanoliter Liquid Volumes in Microfluidic Channels to 40 GHz," IEEE Trans. Instrum. Meas., vol. 59, no. 12, pp. 3279–3288, Dec. 2010.

[2] K. Grenier, D. Dubuc, P.-E. Poleni, M. Kumemura, H. Toshiyoshi, T. Fujii, and H. Fujita, "Integrated Broadband Microwave and Microfluidic Sensor Dedicated to Bioengineering," IEEE Trans. Microw. Theory Tech., vol. 57, no. 12, pp. 3246–3253, Dec. 2009.

[3] S. Liu, I. Ocket, P. Barmuta, A. Lewandowski, D. Schreurs, and B. Nauwelaers, "Broadband dielectric spectroscopy calibration for microliter samples of biogenic liquid," in 2014 44th European Microwave Conference, 2014, pp. 279–282.

[4] J.-C. Chien, M. Anwar, E.-C. Yeh, L. P. Lee, and A. M. Niknejad, "A 1–50 GHz dielectric spectroscopy biosensor with integrated receiver front-end in 65nm CMOS," in 2013 IEEE MTT-S International Microwave Symposium Digest (MTT), 2013, pp. 1–4.

[5] A. Rasmussen, M. Gaitan, L. E. Locascio, and M. E. Zaghloul, "Fabrication techniques to realize CMOS-compatible microfluidic microchannels," J. Microelectromechanical Syst., vol. 10, no. 2, pp. 286–297, Jun. 2001.

[6] H. Lee, Y. Liu, D. Ham, and R. M. Westervelt, "Integrated cell manipulation system - CMOS/microfluidic hybrid," Lab Chip, vol. 7, no. 3, p. 331, Mar. 2007.

[7] J. B. Christen and A. G. Andreou, "Design, Fabrication, and Testing of a Hybrid CMOS/PDMS Microsystem for Cell Culture and Incubation," IEEE Trans. Biomed. Circuits Syst., vol. 1, no. 1, pp. 3–18, Mar. 2007.

[8] E. Ghafar-Zadeh and M. Sawan, "A 0.18 μm CMOS Capacitive Detection Lab-on-Chip," in 2007 IEEE Custom Integrated Circuits Conference, 2007, pp. 165–172.

[9] T. P. Hunt, D. Issadore, and R. M. Westervelt, "Integrated circuit/microfluidic chip to programmably trap and move cells and droplets with dielectrophoresis," Lab Chip, vol. 8, no. 1, pp. 81–7, Jan. 2008.

[10] K. Grenier, D. Dubuc, T. Chen, T. Chretiennot, M. Poupot, and J.-J. Fournie, "Microfluidic on-chip for biomedical applications," in 2011 IEEE Bipolar/BiCMOS Circuits and Technology Meeting, 2011, pp. 129–132.

[11] Y. H. Ghallab and Y. Ismail, “CMOS Based Lab-on-a-Chip: Applications, Challenges and Future Trends,” IEEE Circuits Syst. Mag., vol. 14, no. 2, pp. 27–47, Jan. 2014.

Publications

[1] Y. Ning, X. Ma, C. R. Multari, X. Luo, V. Gholizadeh, C. Palego, X. Cheng, and J. C. M. Hwang, "Improved broadband electrical detection of individual biological cells," in IEEE MTT-S Int. Microwave Symp. Dig., Phoenix, AZ, May. 2015, accepted for publication.

[2] Denzi, C. Merla, C. Palego, A. Paffi, Y. Ning, C. R. Multari, X. Cheng, F. Apollonio, J. C. M. Hwang, and M. Liberti, "Assessment of cytoplasm conductivity by nanosecond pulsed electric fields," IEEE Trans. Biomedical Engineering, accepted for publication.

[3] V. Gholizadeh, Y. Ning, X. Luo, C. Palego, J. C. M. Hwang, and C. L. Goldsmith, "Improved compact, wideband, low-dispersion, metamaterial-based MEMS phase shifters," in IEEE MTT-S Int. Wireless Symp. Dig., Shenzhen, China, Mar. 2015, accepted for publication.

[4] Denzi, F. Apollonio, M. Liberti, C. Merla, Y. Ning, C. Multari, C. Palego, X. Cheng, and J. C. M. Hwang, "Cell detection and discrimination by a microfluidic-integrated broadband microchamber," in Proc. European Microwave Conf., Rome, Italy, Oct. 2014, pp. 695−698.

[5] Y. Ning, C. R. Multari, X. Luo, C. Palego, X. Cheng, J. C. M. Hwang, A. Denzi, F. Apollonio, M. Liberti, and C. Merla, "Reproducible sensing of individual biological cells by broadband microwave signals," in Proc. IEEE Benjamin

Franklin Symp. Microwave Antenna Sub-Systems Radar Telecommunications Biomedical Application, Philadelphia, PA, Sep. 2014, pp. 121−123.

[6] Y. Ning, C. Multari, X. Luo, C. Palego, X. Cheng, J. C. M. Hwang, A. Denzi, C. Merla, F. Apollonio, and M. Liberti, "Broadband electrical detection of individual biological cells," IEEE Trans. Microwave Theory Techniques, vol. 62, no. 9, pp. 1905−1911, Sep. 2014.

[7] C. Multari, Y. Ning, X. Luo, C. Palego, A. Denzi, C. Merla, F. Apollonio, M. Liberti, J. C. M. Hwang, and X. Cheng, "Cell detection by a microfluidic-integrated broadband biosensor," in Proc. NTSI-Nanotech Conf., National Harbor, MD, Jun. 2014, vol. 2, pp. 101−104.

[8] Denzi, C. Merla, C. Palego, Y. Ning, C. Multari, X. Cheng, F. Apollonio, J. C. M. Hwang, and M. Liberti, "An improvement method of estimation for cell cytoplasm conductivity using nanosecond pulsed electrical fields: coupling of a microdosimetric model with experiments for a single cell," in Proc. BioEM Conf., Cape Town, S. Africa, Jun. 2014, pp. 385−388.

[9] C. Palego, Y. Ning, V. Gholizadeh, X. Luo, J. C. M. Hwang, and C. L. Goldsmith, "Compact, wideband, low-dispersion, metamaterial-based MEMS phase shifters," in IEEE MTT-S Int. Microwave Symp. Dig., Tampa, FL, Jun. 2014, pp. 1−4

[10] Y. Ning, C. R. Multari, X. Luo, C. Merla, C. Palego, X. Cheng, and J. C. M. Hwang, "Fast, compact and label-free electrical detection of live and dead single cells," in Proc. IEEE Int. Microwave Workshop Series RF Wireless Technologies Biomedical Healthcare Applications, Singapore, Dec. 2013, pp. 1−3.

[11] Y. Ning, C. Multari, X. Luo, C. Palego, D. Molinero, X. Cheng, J. C. M. Hwang, and C. Merla, "Coplanar stripline microchamber for electrical detection of live and dead biological cells," in Proc. European Microwave Conf., Nuremberg, Germany, Oct. 2013, pp. 475−478.

[12] Denzi, C. Merla, C. Palego, Y. Ning, F. Apollonio, J. C. M. Hwang, and M. Liberti, "Microdosimetric model of a single cell for nanosecond pulsed electric fields: an experimental method of validation," in Proc. BioEM Conf., Thessaloniki, Greece, Jun. 2013, pp. 655-659.

[13] X. Luo, Y. Ning, D. Molinero, C. Palego, J. C. M. Hwang, and C. L. Goldsmith, "Intermodulation distortion of actuated MEMS capacitive switches," in IEEE Automated RF Techniques Group Conf. Dig., Seattle, WA, Jun. 2013, pp. 1−3.

[14] D. Molinero, C. Palego, X. Luo, Y. Ning, G. Ding, J. C. M. Hwang, and C. L. Goldsmith, "Intermodulation distortion in MEMS capacitive switches under high RF power," in IEEE MTT-S Int. Microwave Symp. Dig., Seattle, WA, Jun. 2013, pp. 1−3.

[15] C. Palego, C. Merla, Y. Ning, C. R. Multari, X. Cheng, D. G. Molinero, G. Ding, X. Luo, and J. C. M. Hwang, "Broadband microchamber for electrical detection of live and dead biological cells," in IEEE MTT-S Int. Microwave Symp. Dig., Jun. 2013, pp. 1−3.

[16] C. Palego, D. Molinero, Y. Ning, X. Luo, J. C. M. Hwang, and C. L. Goldsmith, "Pull-in and release transients of MEMS capacitive switches under high RF power,"

in Proc. European Microwave Integrated Circuits Conf., Oct. 2012, Amsterdam, Netherlands, pp. 437−440.

Vita

Yaqing Ning was born on August 8, 1988 in Tianjin, China, the daughter of Jinling Cao and Jinwei Ning. She received the B.S. degree in Electrical Engineering from Shanghai Jiao Tong University, Shanghai, China, in 2010. She studied at Department of Electrical Engineering at Lehigh University, Bethlehem, PA, and pursued her PhD degree under the guidance of Prof. James C.M. Hwang. During her stay at Lehigh University, she had been awarded the Sherman Fairchild Fellowship in Solid State Studies for three consecutive years from 2012 to 2014. She was a summer intern with RF Micro Devices, Inc., Greensboro, NC, in 2013, where she was involved with device modeling and electromagnetic simulation for linearity improvement through RF characterization. Her current research interests include electrical detection for biological cell, RF semiconductor, MEMS capacitive switch and phase shifter.